

Vadman, M.J., Garvue, M.M., Spotila, J.A., Bemis, S.P., Stamps, D.S., Owen, L.A., and Figueiredo, P.M., 2023, Evidence for a prehistoric multifault rupture along the southern Calico fault system, Eastern California Shear Zone, USA: *Geosphere*, v. 19, <https://doi.org/10.1130/GES02653.1>

**Supplemental Material, Part A: Additional Figures and Information**

**“Evidence for a Prehistoric Multifault Rupture Along the Southern Calico Fault System, Eastern California Shear Zone, USA”**

**Vadman et al., 2023**

**Geosphere  
6/4/2023**

### **Note on author contributions to the manuscript:**

For questions regarding the methods, results, and interpretations in this manuscript, note that the two senior authors contributed as follows:

Michael Vadman: Directed paleoseismic trenching and interpretation, conducted Coulomb modeling of the paleorupture scenarios, produced Figures 1, 4, 7, 8, 10, 11, S2, S5, S6, Table 2, assisted in age interpretation and Supplement Part C, wrote paragraphs associated with the paleoseismic and Coulomb methods, observations, and interpretations.

Max Garvue: Directed the paleorupture mapping and offset measurements (field and remote mapping), lead observations and interpretations of the expression and character of the paleorupture, produced Figures 2, 3, 5, 6, 9, 12, S1, S3, S4, Supplemental Material Part B, and Table 2, calculated COPD and along strike average offsets, acquired and performed terrestrial-based photogrammetry to produce the SfM DEM in Figure 5, wrote paragraphs associated with the paleorupture methods, observations, and interpretations.



**Figure S1:** Example satellite and field images of an old, possible prehistoric, footpath along the east flank of Hidalgo Mountain (see Figure 2 for location). Upper figure shows an interpreted footpath in satellite images (upper is uninterpreted, lower shows interpreted footpaths in dashed white lines, which are thicker where more obvious). Field images below correspond to locations A and B. Note that the footpath appears as a trough with a light gray center line and two darker outer lines in the satellite image, rather than a white lineament. The trace of the path also follows a contour, contours in and out of gullies, and curves to avoid obstacles. In the field, the interpreted path appears person-wide and is hard packed, not soft and disaggregated like the interpreted paleorupture. White lines define interpreted limits of the path in photos. Although the age of this interpreted path is unknown, this location is currently closed to the public and may thus reflect foot traffic associated with military training. Given training-related paths are short and extend between strategic sites, and that long-distance travel is completed by vehicles, it is possible that the path is older. Military training has been conducted in this area for 80 years, so the path may reflect repeated foot traffic prior to this, related to mining or earlier travel by Indigenous People that inhabited the Mojave as far back as 10 ka.





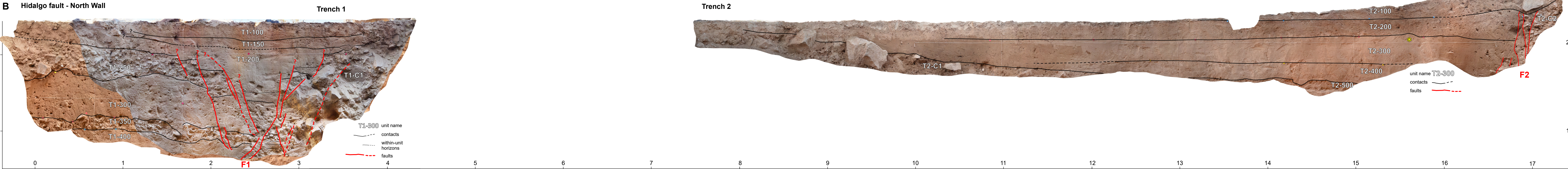
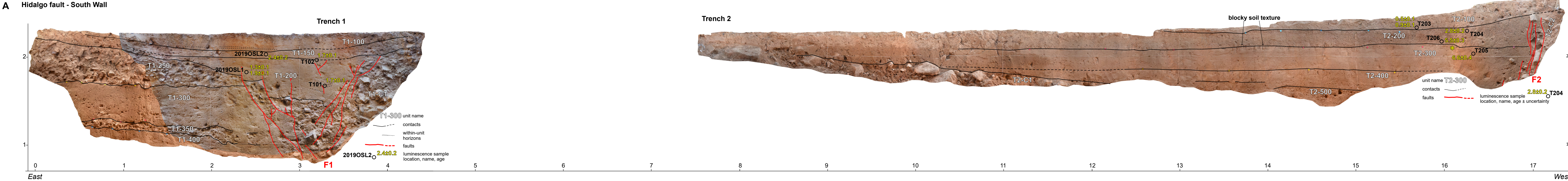
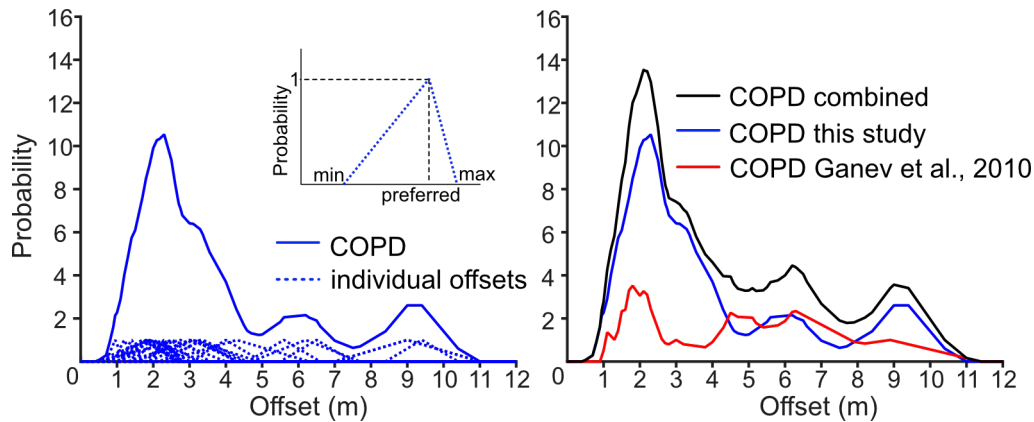


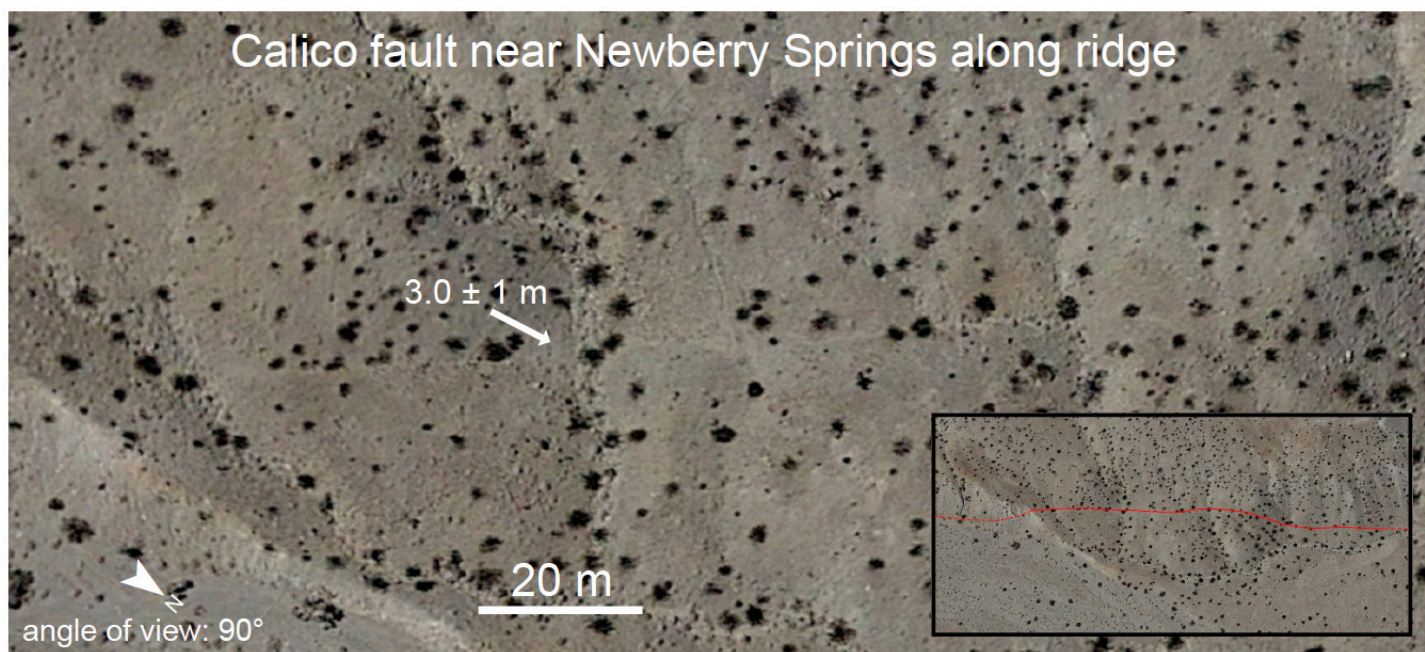
Figure S2. South (A) and north (B) walls of the paleoseismic trenches across the Hidalgo fault. We have positioned Trench 1 and Trench 2 for each wall at their appropriate horizontal and vertical positions. The north wall has been flipped horizontally so that it is displayed in the same perspective as the south wall. The ground surface of the unexcavated zone between trenches 1 and 2 consisted of very coarse-grained, bouldery deposits similar to the exposures of units T1-C1 and T2-C1.



**Figure S3:** Cumulative Offset Probability Distribution (COPD) for dextral displacement measurements on the Calico-Hidalgo paleorupture using normalized probabilities for individual measurements (i.e., normalized to probability height of 1). This alternative calculation method to the COPD shown in Figure 9 yields a comparable result, but treats offsets equally given that each was of comparable high quality. This shows that embedding assumptions about measurement quality into the COPD calculation does not affect the magnitude of the main peak. Solid blue line is the summed COPD for individual triangular distributions of individual measurements, which are shown as dashed blue lines. A visual explanation of triangular distributions is shown in the upper right. The tallest peak on the COPD is interpreted as the representative displacement of the most recent event, whereas shorter peaks at higher displacement may represent multiple events.



**Figure S4:** The trace of the Calico fault surface expression near New Berry Springs in the vicinity of the Ganey et al. (2010) paleoseismic site. Ganey et al. (2010) measured offsets along this segment of the fault, as synthesized in Figure 9. Upper plot shows Google Earth satellite image of the fault, which is expressed as a white lineament and appears very similar to the lineament interpreted as a paleorupture along the combined Calico-Hidalgo fault in this study, as well as to the trace of the 1999 Hector Mine rupture and other potential paleoruptures on the Lenwood and Humbug Mountain faults (compare to Figures 3, 12). Center of upper image is 34.75805°N, 116.61117°W. Lower image shows another location along the Calico fault near Newberry Springs in both satellite (left) and lidar (right). Note that the fault here occurs at a releasing bend and has a significant vertical component. Center of lower image is 34.78734°N, 116.63707°W. Offsets measured by Ganey et al. (2010) are indicated in both images.



satellite

lidar

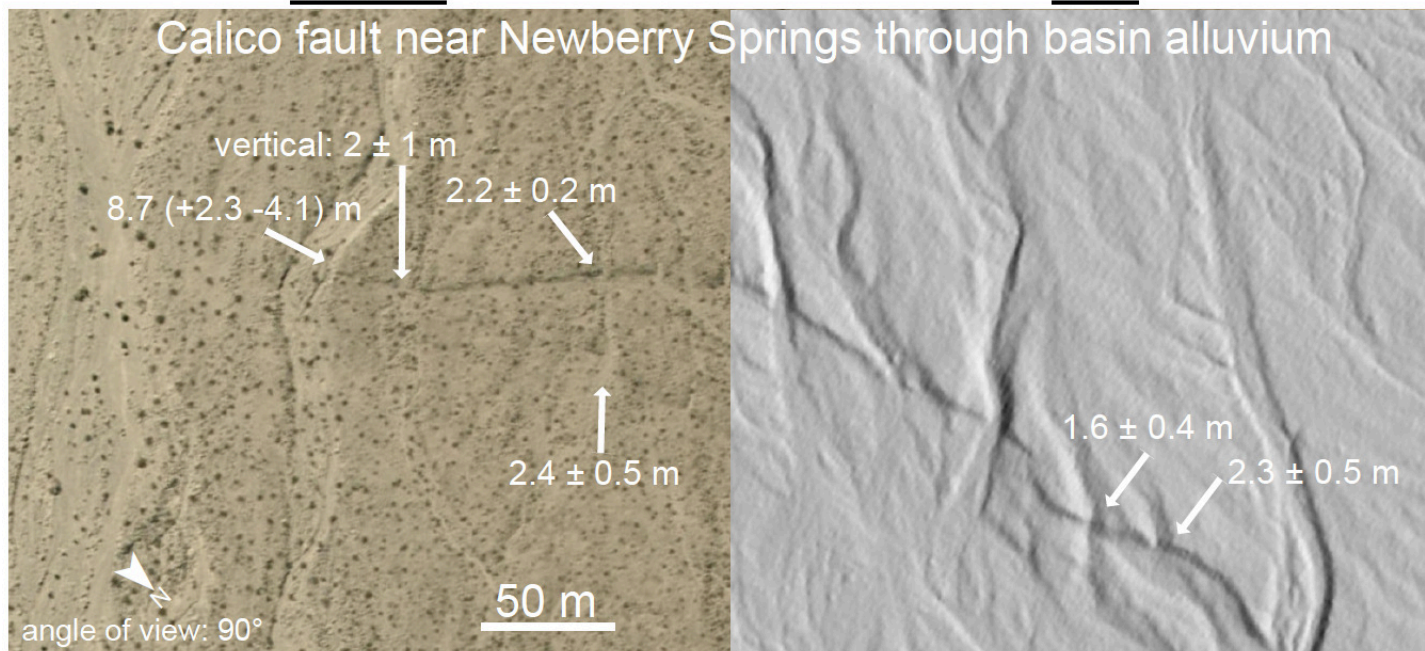




**Figure S5:** Maps showing each rupture scenario extent and slip used for Coulomb modeling. For each scenario shown, tests for coefficients of friction of 0.20, 0.40, and 0.60 were run. The rupture for each scenario is colored red for full slip or pink where it is partitioned across multiple strands. Scenario A has a rupture length of 16.7 km, a fault depth of 10 km and slip of 2.3 m. Scenario B has a rupture length of 20.5 km and fault depth of 10 km. It has a slip of 2.3m, partitioned in half with overlapping strands each slipping 1.15 m. Scenario C has a rupture length of 62.5 km, a fault depth of 10 m, and slip of 2.3 m. Scenario D has a rupture length of 88.8 km. We tested both variable fault depth (10 and 18 km) and variable slip (2.3 and 5 m). Scenario E has a rupture length of 112.3 km. Similar to scenario D, we tested both variable fault depth (10 and 18 km) and variable slip (2.3 and 5 m). Where there are overlapping strands, we partitioned that slip into the respective halves of 1.15 m or 2.5 m.

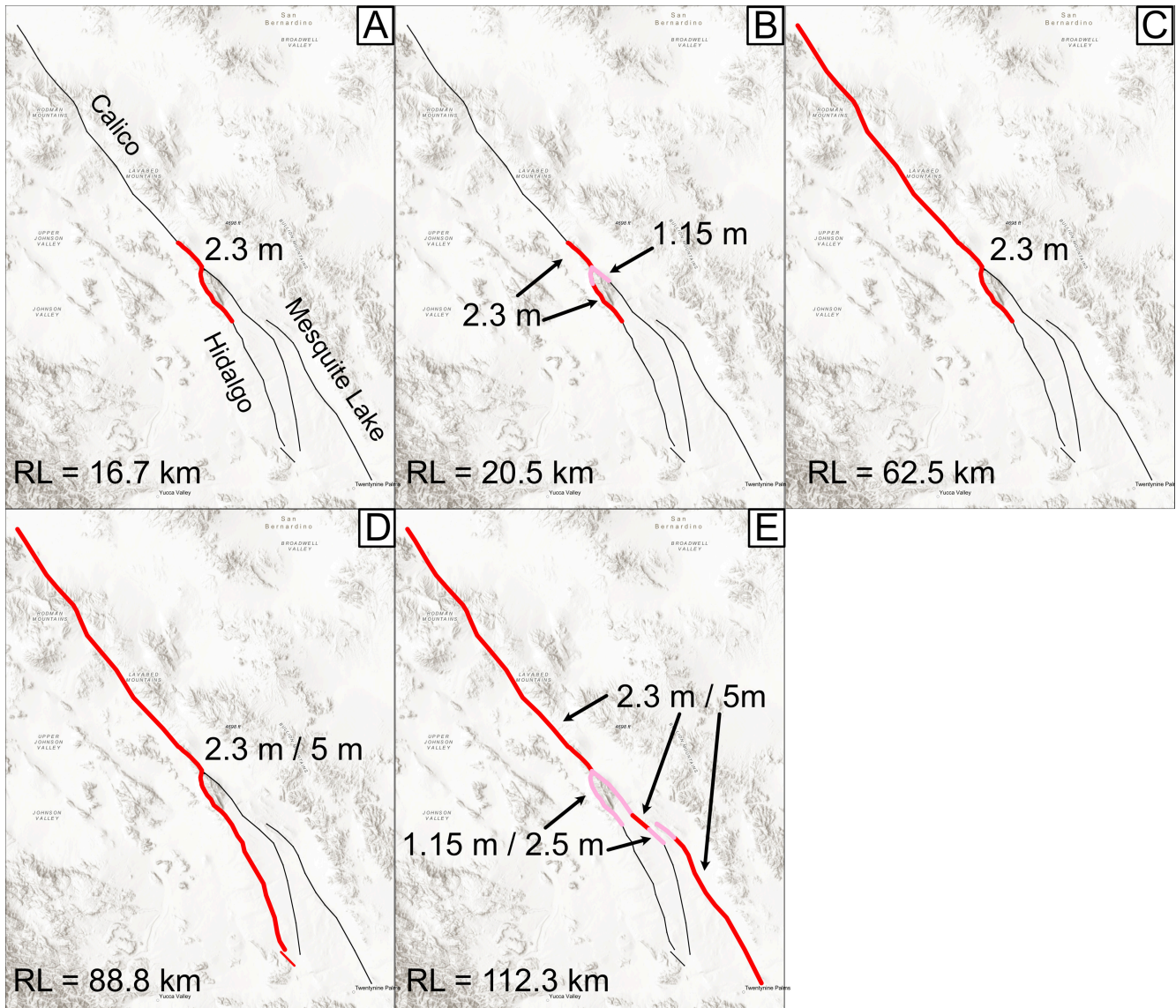


**Figure S6a:** Results of Coulomb CFF modeling for Scenarios A, B, and C (shown in Figure S5). Model parameters including scenario, coefficient of friction, rupture length, depth of fault, and amount of slip are labeled in lower right of each diagram. Text in lower left indicates whether the scenario resulted in a positive  $\Delta\text{CFF}$  at the location of the 1992 Landers and 1999 Hector Mine (with depths of 7 and 15 km test) hypocenters. For example, Scenario A with  $\mu=0.4$  resulted in  $+\Delta\text{CFF}$  for the Hector Mine hypocenters of 7 and 15 km, but not the 1992 Landers hypocenter.

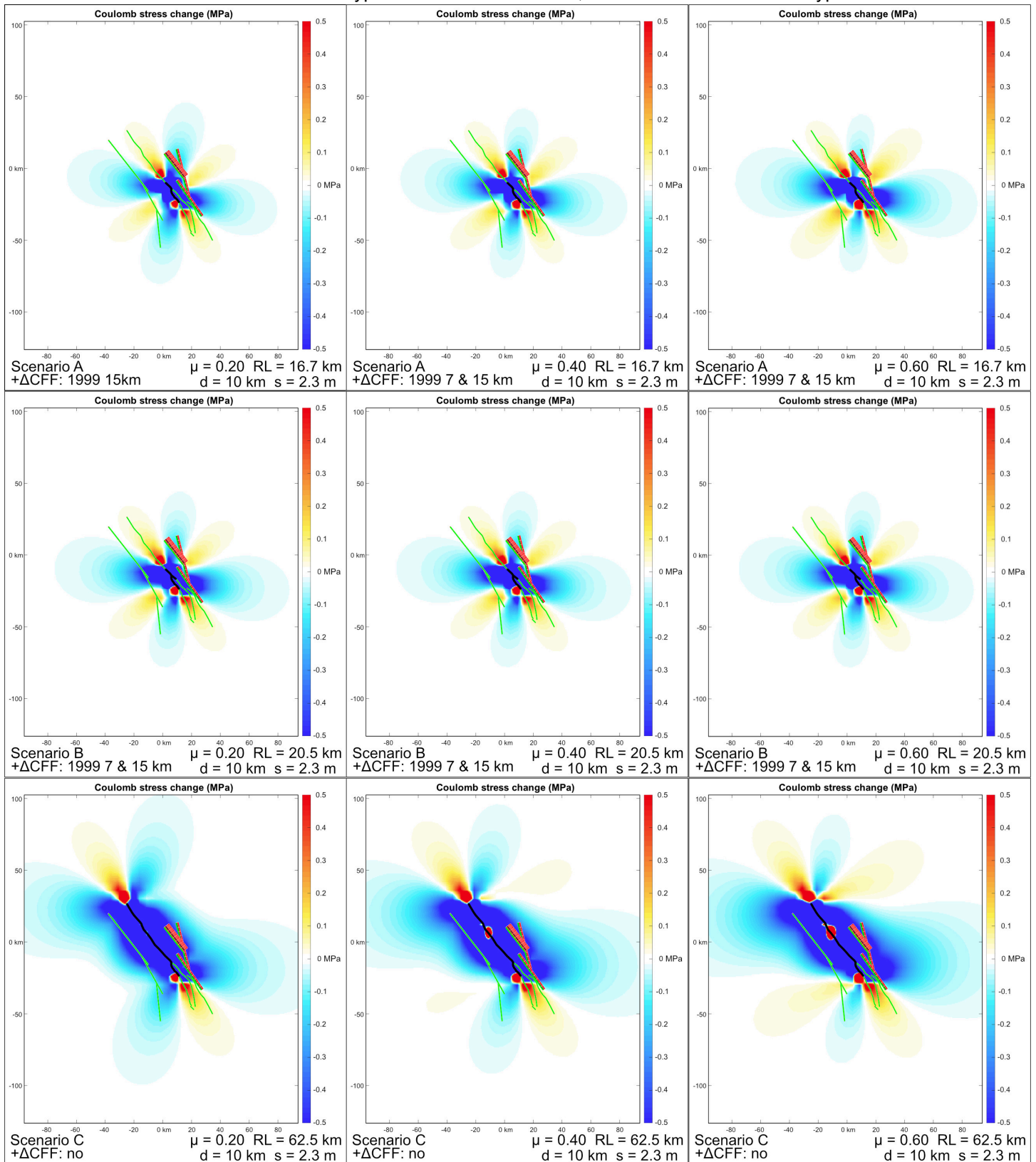




**Figure S6b:** Results of Coulomb CFF modeling for Scenario D (shown in Figure S5). All else as in Figure S6a.

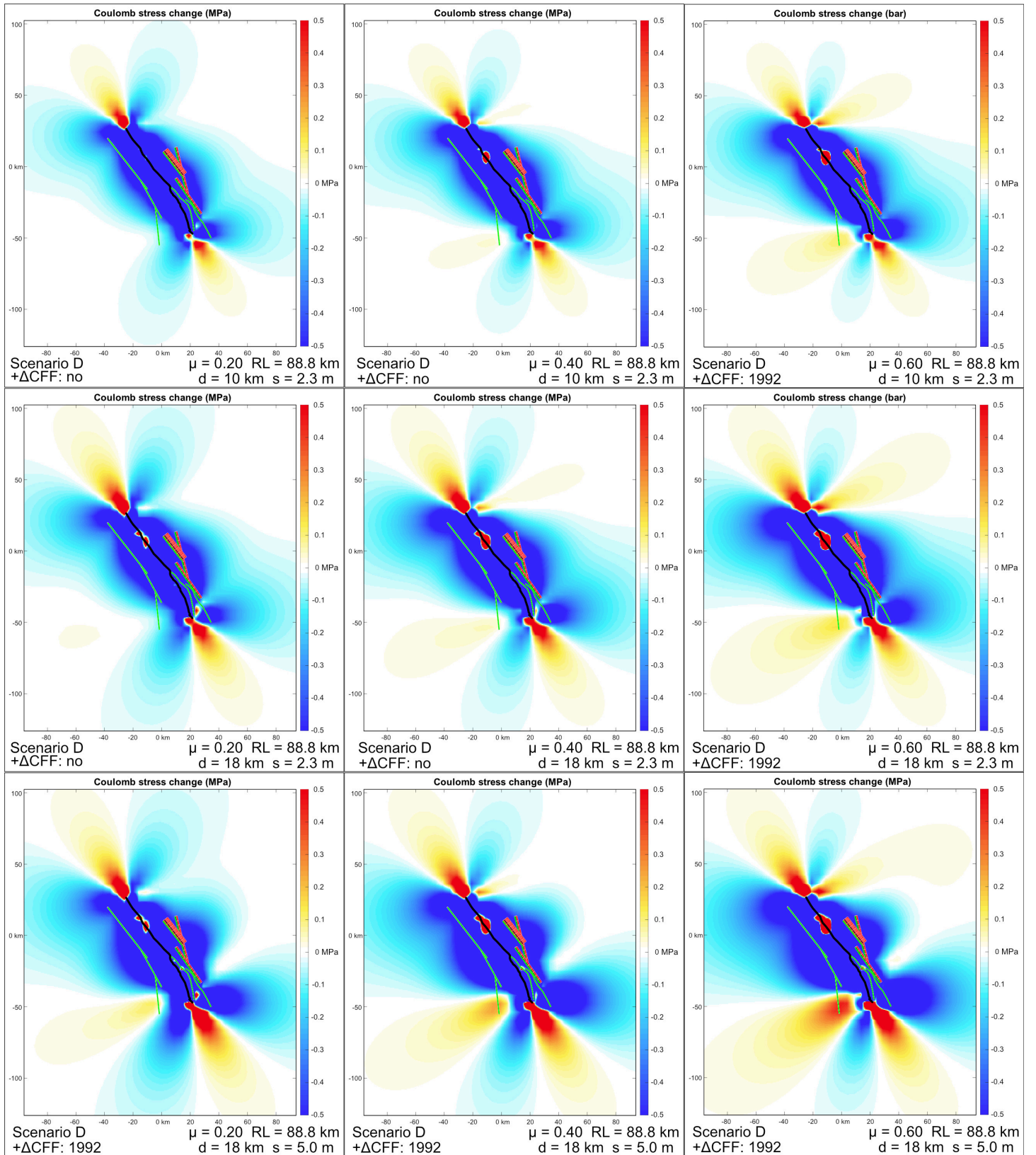
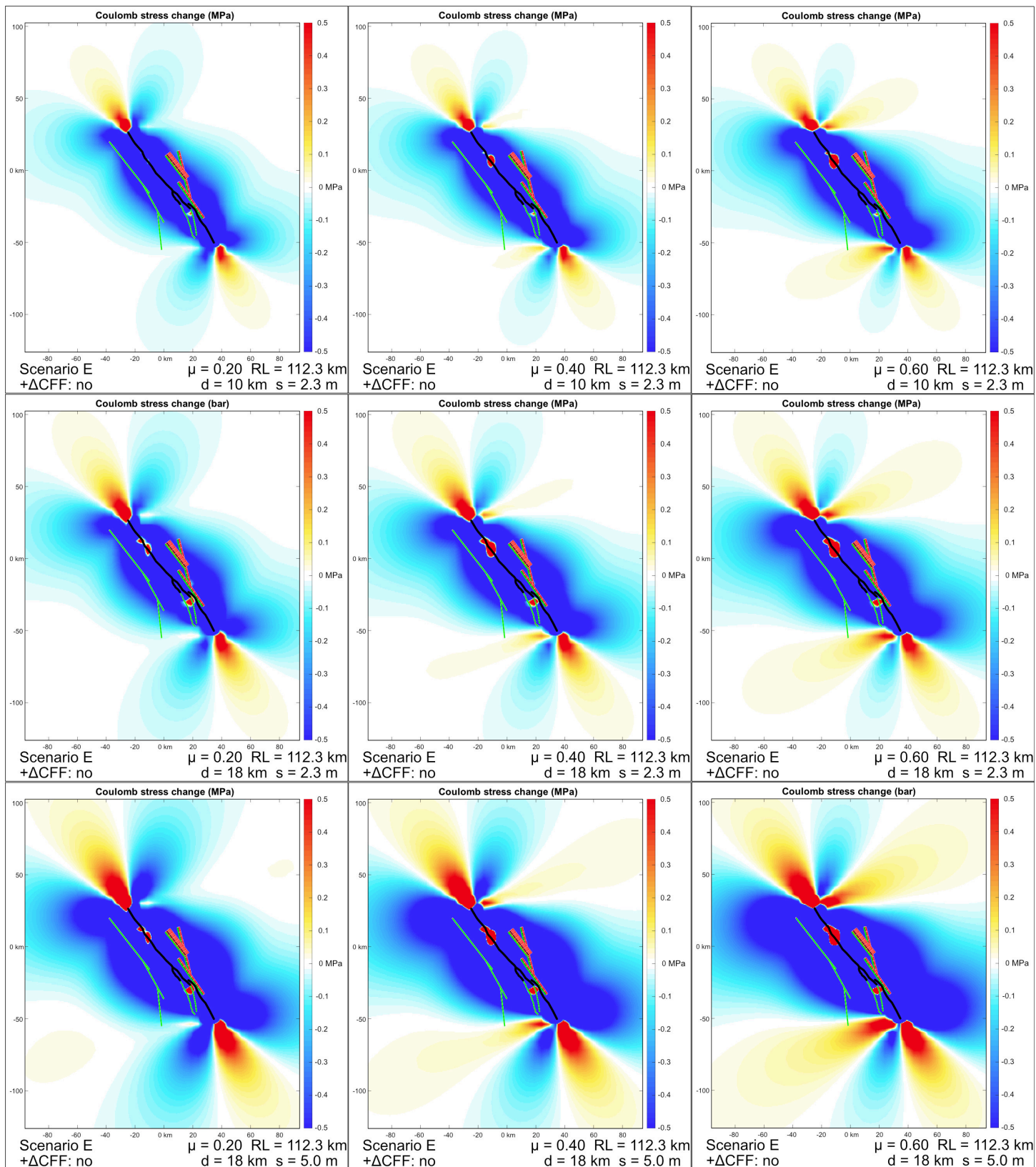


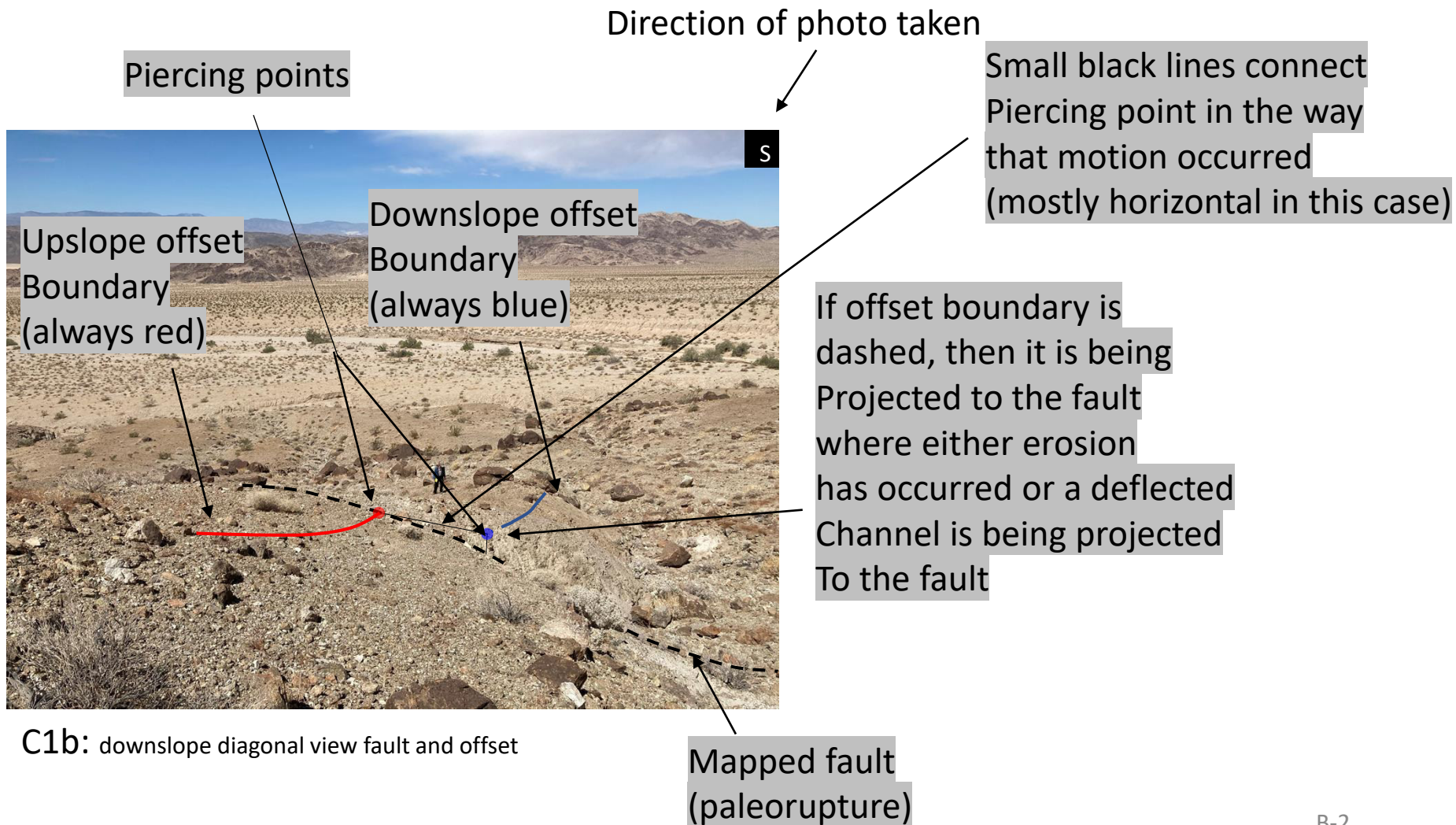
**Figure S6c:** Results of Coulomb CFF modeling for Scenario E (shown in Figure S5). All else as in Figure S6a.



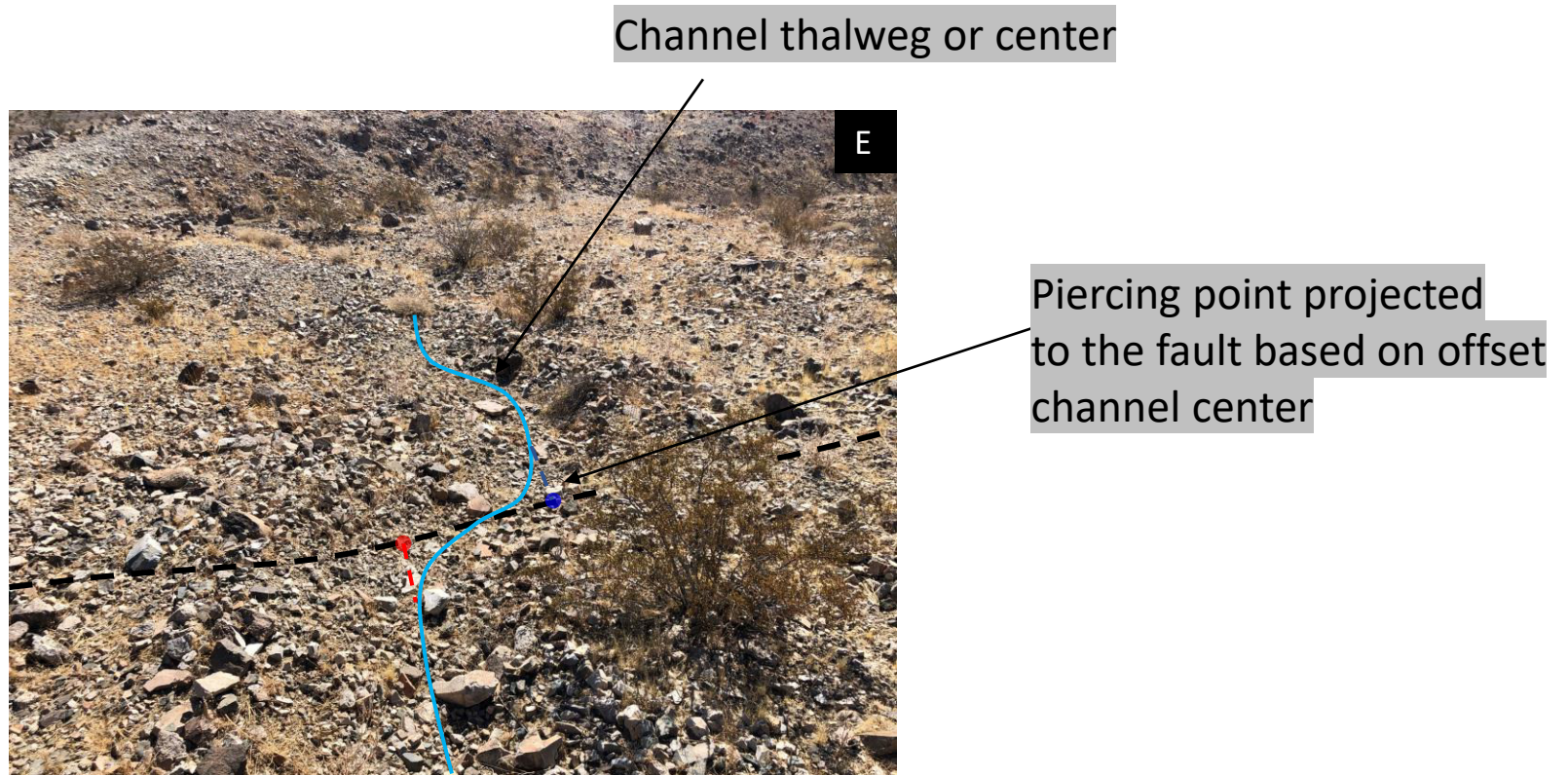


**Supplemental Material, Part B: Measured offsets along the  
Calico-Hidalgo paleorupture.**

# example 1



# example 2

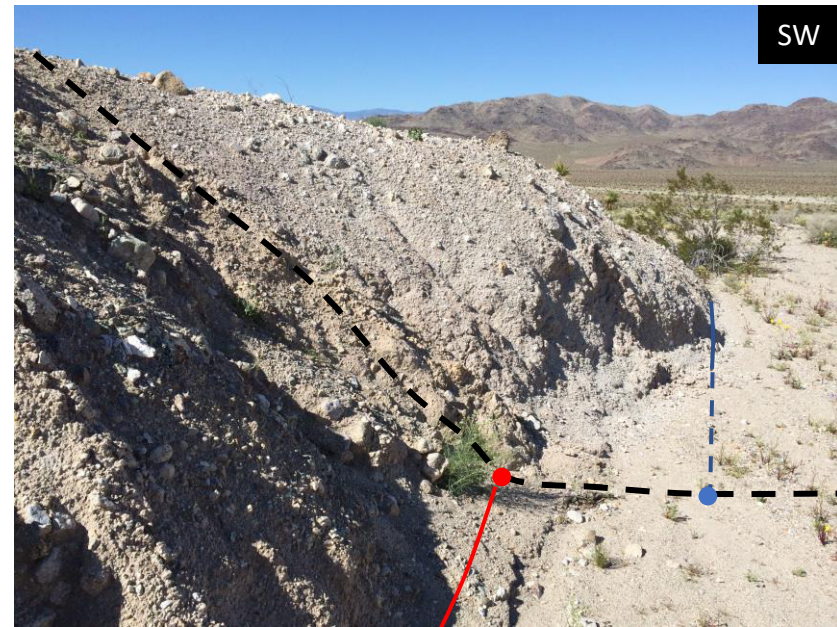


C19b:



# C1\*

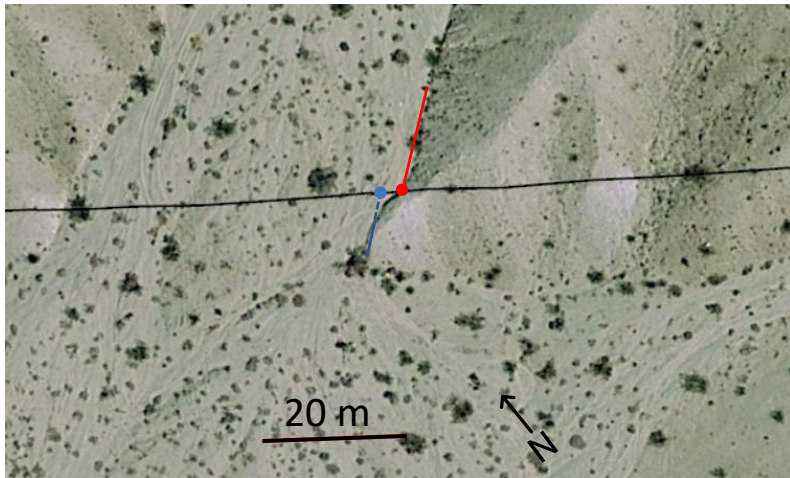
Coordinates (Lat Lon)	34.51678°, -116.38653°
Horizontal Dextral Offset (m)	1.90 +1.00, -0.50 m (shutter ridge)
Method of Measurement	Tape measure
Site Description and Uncertainty	Shutter ridge on the south side of large drainage. Piercing points were based on the offset from the inside edge of the drainage to the outer erosional margin of the shutter. An uncertainty of +1.00 -0.50 m was assigned due sloughing and erosional morphology. * - not included in slip distribution or COPD (occurs on uncertain trace)
Age Interpretation	Most recent event



C1b



C1c



C1a

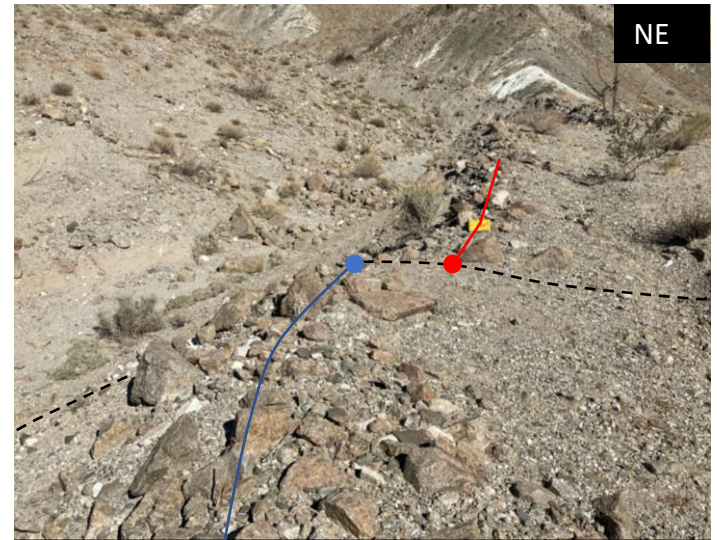


## C2

Coordinates (Lat Lon)	34.50443°, -116.37144°
Horizontal Dextral Offset (m)	1.20 ± 0.30 m (riser margin)
Method of Measurement	Tape measure
Site Description and Uncertainty	Offset riser margin of preserved alluvial surface between two active drainages. Two parallel fault strands are clearly exposed in the south wall of the large channel. Offset is aligned with the eastern fault strand. Uncertainty of ± 0.30 m was assigned due to the erosional slope of the riser margin.
Age Interpretation	Most recent event



C2a



C2b

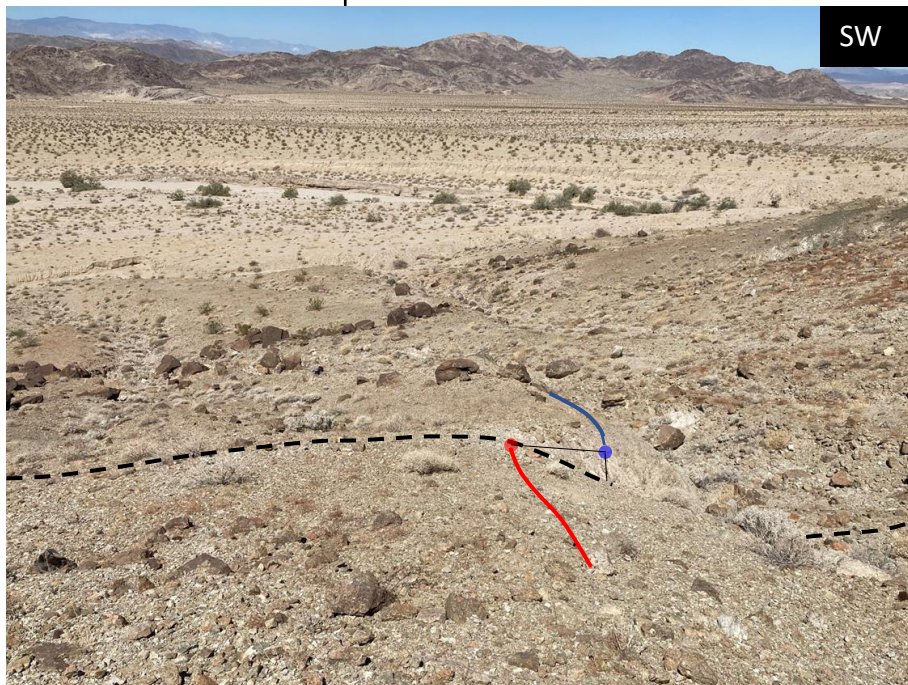


C2c

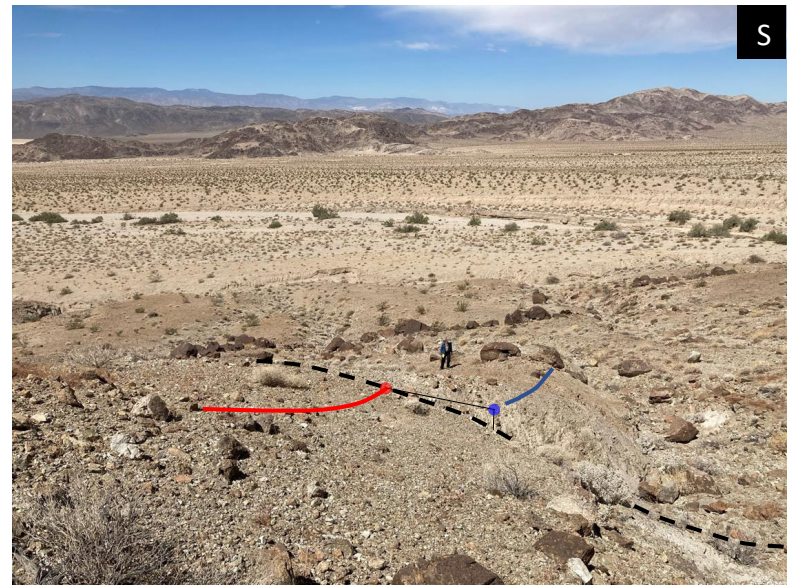


## C3''

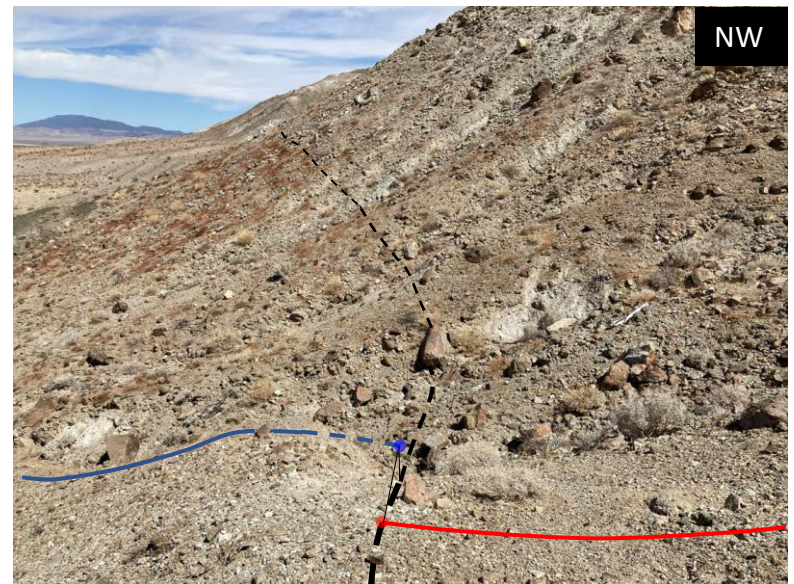
Coordinates (Lat Lon)	34.50348°, -116.37046°
Horizontal Dextral Offset (m)	2.0 ± 1.0 m (displaced margin of shutter panel)
Method of Measurement	" - By eye and the Google Earth measuring tool. Did not measure with tape due time constraints.
Site Description and Uncertainty	Shutter ridge with a trough that gullies NW into the drainage. Piercing points and lines represent the displaced riser margin and could both be moved 0.5 m to the NW or SE.
Age Interpretation	Most recent event



C3a



C3b



C3c



### C3''

Coordinates (Lat Lon)	34.50348°, -116.37046°
Horizontal Dextral Offset (m)	2.0 ± 1.0 m (displaced margin of shutter panel)
Method of Measurement	" - By eye and the Google Earth measuring tool. Did not measure with tape due time constraints.
Site Description and Uncertainty	Shutter ridge with a trough that gullies NW into the drainage. Piercing points and lines represent the displaced riser margin and could both be moved 0.5 m to the NW or SE.
Age Interpretation	Most recent event



C3e

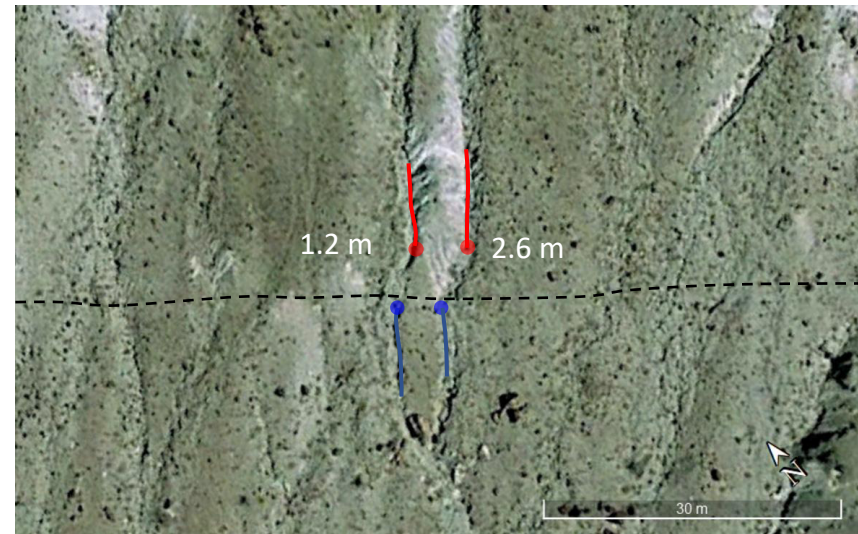


C3d



## C4''

Coordinates (Lat Lon)	34.503070°, -116.369975°
Horizontal Dextral Offset (m)	1.9 + 1.5 m (average)  1.2 ± 0.8 (NW channel thalweg) 2.6 ± 0.8 (SE channel thalweg)
Method of Measurement	" - By eye and the Google Earth measuring tool. Did not measure with tape in the field due to time constraints.
Site Description and Uncertainty	Deflected channels were measured on NW and SE side of the down sloping spur ridge. The spur rises NE of the fault and consists of chewed up felsic and mafic dikes. The surface of the spur on the SW side of fault is preserved alluvium and is bounded by the deflected channels. The uncertainty of the average offset is from the min and max limits of the deflected channels which are given due to the resolution of the Google Earth imagery
Age Interpretation	Most recent event



C4a



C4b

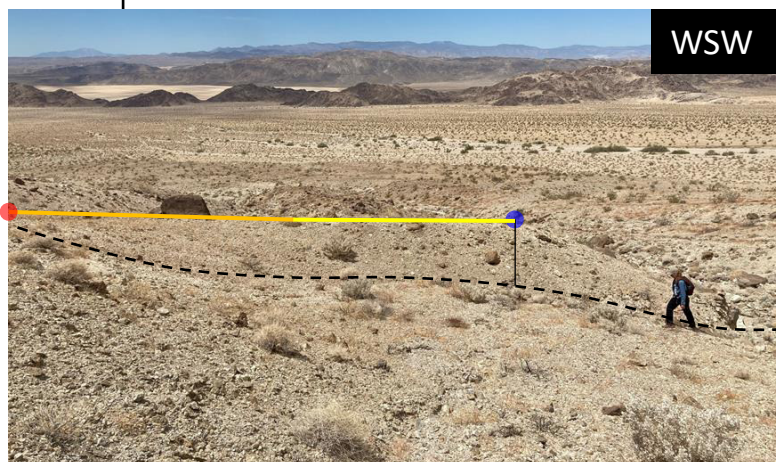


## C5^

Coordinates (Lat Lon)	34.50211°, -116.36865°
Horizontal Dextral Offset (m)	9.00 ± 2.00 m (shutter ridge)
Method of Measurement	Tape measure
Site Description and Uncertainty	<p>Sharp and striking shutter ridge with a level ridge surface. The piercing points represent the displaced riser margin. The uncertainty is based on the placement of the NW termination of the shutter ridge due to erosion and material sloughing. The offset likely represents both the most recent and penultimate events. The penultimate event could be represented by the NW 4 m section (yellow) that is more irregular and eroded, while the SE 5 m section (orange) is somewhat sharper.</p> <p>^ - not included in slip distribution graph (possibly multiple events)</p>
Age interpretation	Multiple events



C5b



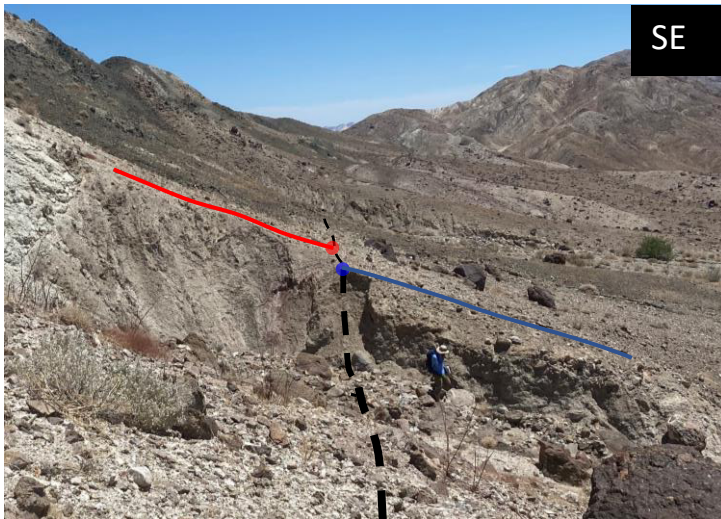
C5a

## C6''

Coordinates (Lat Lon)	34.50015°, -116.36554°
Horizontal Dextral Offset (m)	2.0 ± 1.0 m (upper riser margin)
Method of Measurement	" - By eye and the Google Earth measuring tool. Did not measure with tape in the field due to rough terrain.
Site Description and Uncertainty	Displaced upper margin of large drainage wall with subtle break in slope on fault that corresponds to a change in drainage wall morphology. Blue piercing point and line was placed on the inward edge of where the colluvial drape juts out and slopes down to the NW. The red piecing point and line were placed on the upslope corresponding margin but has no persevered colluvium drape. The uncertainty is based on the rough estimate by eye and the resolution available in Google Earth
Age interpretation	Most recent event



C6b



C6a



## C7

Coordinates (Lat Lon)	34.49974°, -116.36506°
Horizontal Dextral Offset (m)	5.60 ± 1.00 m (drainage edge)
Method of Measurement	Tape measure
Site Description and Uncertainty	<p>Abrupt widening at the outlet of the NW drainage edge where the base of the fan rises from the active drainage (blue line) on the SSW side of the fault and where bedrock emerges from the active drainage on the NNE side of the fault.</p> <p>The piercing points could be moved 50 cm in either direction along the fault due to erosional slopes of drainage edge.</p>
Age interpretation	Most recent event and maybe penultimate event



C7b



C7a



## C8^"

Coordinates (Lat Lon)	34.499038°, -116.363732°
Horizontal Dextral Offset (m)	9.0 ± 2.0 m (channel thalweg)
Method of Measurement	" - The Google Earth measuring tool. Did not measure with tape in field due to time constraints.
Site Description and Uncertainty	Deflected channel from dextrally displaced pressure ridge of an old landslide unit on the piedmont. Ground is soft and churned underfoot and corresponds to a sharp contact of bedrock to pressure ridge unit. The uncertainty is based on the available resolution of Google Earth imagery. ^ - not included in slip distribution graph (possibly multiple events)
Age interpretation	Multiple events



C8b

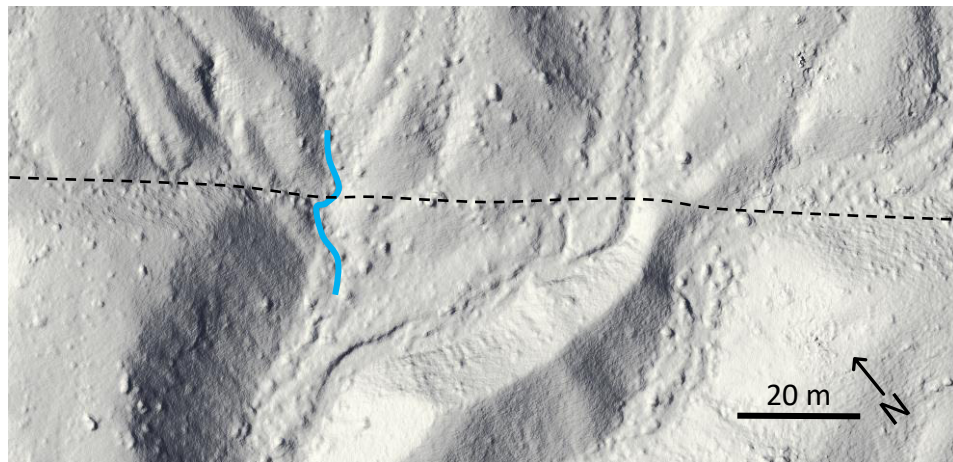


C8a



## C9

Coordinates (Lat Lon)	34.495618°, -116.359168°
Horizontal Dextral Offset (m)	$1.80 \pm 1.00$ m (average) $1.70 \pm 0.70$ m (thalweg) $1.60 \pm 0.80$ m (south edge of channel) $2.15 \pm 0.70$ m (upper margin of shutter ridge panel)
Method of Measurement	Tape measure
Site Description and Uncertainty	Channel deflected by small colluvium shutter ridge along sharp narrow zone of disturbance. The uncertainty is based on the minimum and maximum offsets from the error bars of the piercing points of the 3 measured features.
Age interpretation	Most recent event



C9a



C9b: upper margin of shutter ridge panel



C9c: upper margin of shutter ridge panel

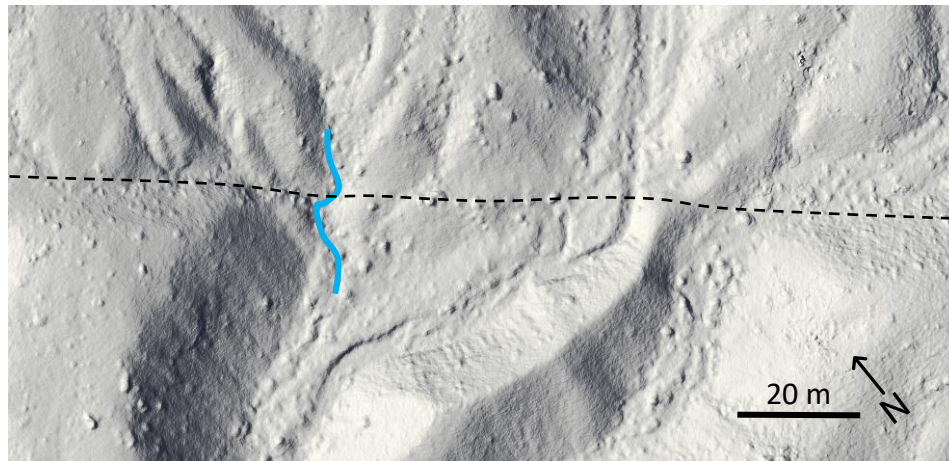
NNE

W



## C9

Coordinates (Lat Lon)	34.495618°, -116.359168°
Horizontal Dextral Offset (m)	$1.80 \pm 1.00$ m (average) $1.70 \pm 0.70$ m (thalweg) $1.60 \pm 0.80$ m (south edge of channel) $2.15 \pm 0.70$ m (upper margin of shutter ridge panel)
Method of Measurement	Tape measure
Site Description and Uncertainty	Channel deflected by small colluvium shutter ridge along sharp narrow zone of disturbance. The uncertainty is based on the minimum and maximum offsets from the error bars of the piercing points of the 3 measured features.
Age interpretation	Most recent event



C9a:



C9d: south edge of channel

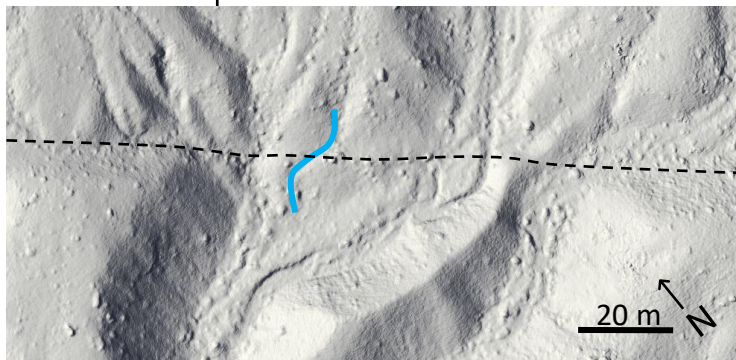


C9e: south edge of channel



## C10<sup>^</sup>

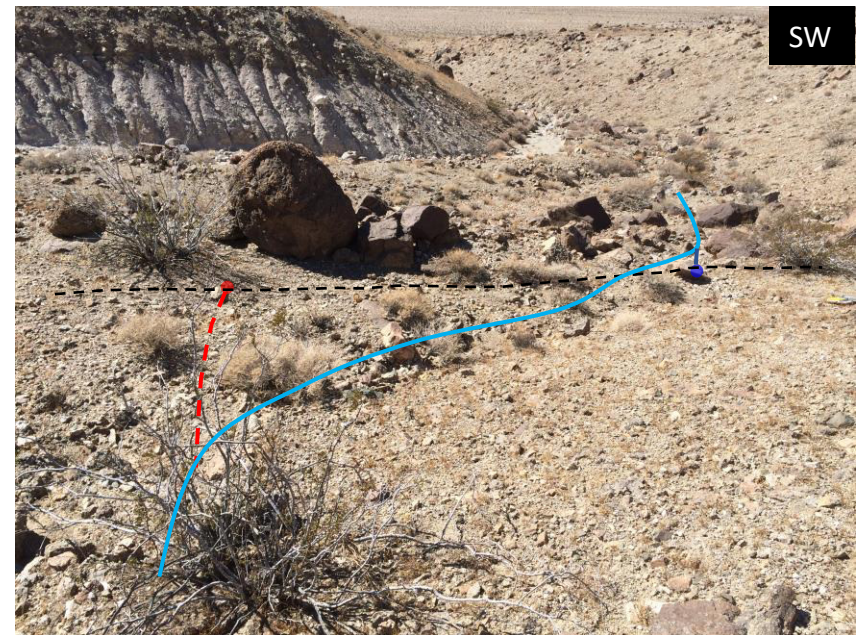
Coordinates (Lat Lon)	34.495553°, -116.359100°
Horizontal Dextral Offset (m)	6.20 ± 1.50 m (average)  6.45 ± 1.00 m (thalweg) 5.80 ± 1.00 m (south channel edge) 6.50 ± 1.00 m (north channel edge)
Method of Measurement	Tape measure
Site Description and Uncertainty	Deflected drainage a few meters south of C9. Shutter ridge is less defined here and therefore was not measured, but the continuation of the narrow zone of flat disturbance that defines the fault is sharp here as well. The uncertainty is given based on the natural channel edge variations that make it difficult to define precisely. ^ - not included in slip distribution graph (possibly multiple events)
Age interpretation	Multiple events



C10a



C10b

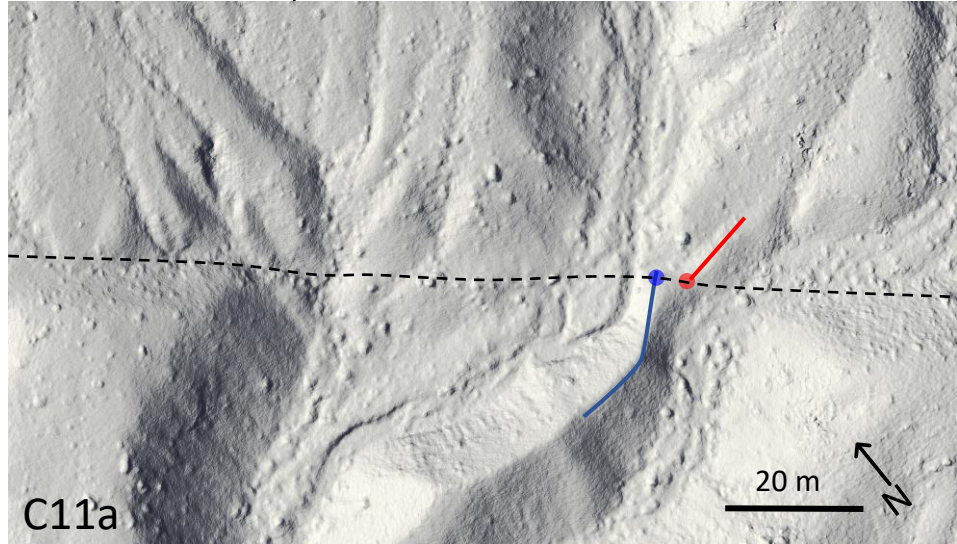


C10c



# C11

Coordinates (Lat Lon)	34.495289°, -116.358767°
Horizontal Dextral Offset (m)	$4.00 \pm 1.00$ m (average) $3.90 \pm 1.00$ m (north facing offset ridge panel) $3.35 \pm 0.50$ (south facing offset ridge panel) $4.75 \pm 0.40$ m (apex of ridge)
Method of Measurement	Tape measure
Site Description and Uncertainty	Offset ridge. The ridge is different material on either side of the fault, but a single geomorphic feature produced by gully erosion on either flank. Uncertainty offset measurements based on gullying and erosion on both flanks.
Age interpretation	Most recent event



C11b

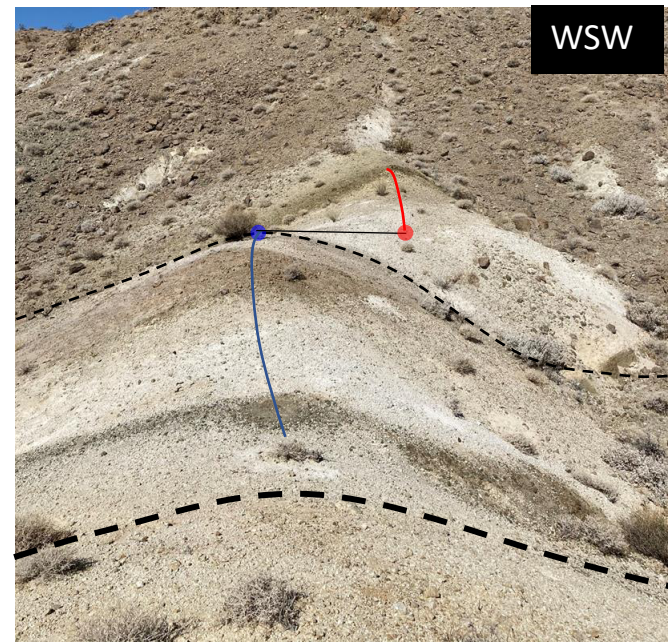


C11c

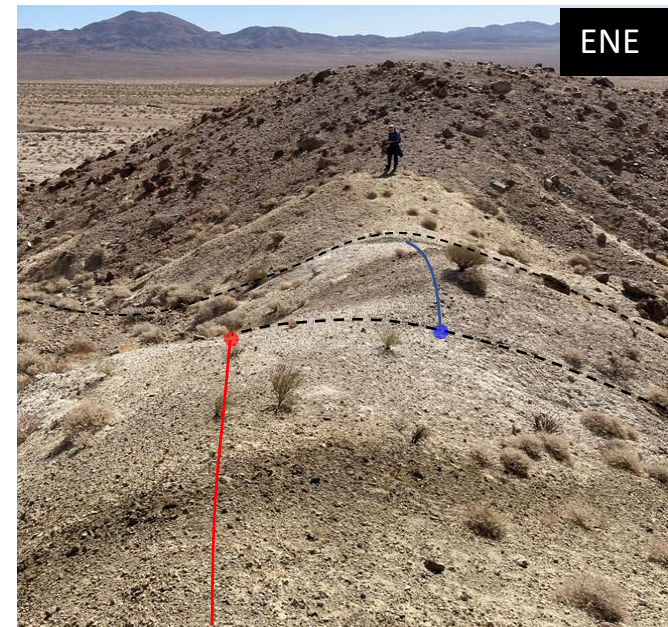


## C12\*

Coordinates (Lat Lon)	34.495766°, -116.354174°
Horizontal Dextral Offset (m)	4.0 ± 1.2 m (apex of the ridge)
Method of Measurement	Paced out due to time constraints.
Site Description and Uncertainty*	<p>A higher degree of speculation is given to this offset as it is not as striking and fresh as other features meaning it may be older than the MRE. Offset ridge of erodible and chewed up bedrock dikes within a larger saddle feature that includes channels on either side which lead to larger drainages. The piercing points and colored lines represent the displaced apex of the ridge which were roughly estimated by pacing out the distance. A large uncertainty is given based on the rough method of estimation even though the ridge crest is quite narrow.</p> <p>* - not included in slip distribution or COPD (occurs on uncertain trace)</p> <p>Note: A second fault strand without measurable offset is ~6 m to the ENE and evidenced by several small knobs, saddles, and linear features to the north and south</p>
Age interpretation	Most recent event with speculation



C12b



C12a

## C12\*

Coordinates (Lat Lon)	34.495766°, -116.354174°
Horizontal Dextral Offset (m)	4.0 ± 1.2 m (apex of the ridge)
Method of Measurement	Paced out due to time constraints.
Site Description and Uncertainty*	<p>A higher degree of speculation is given to this offset as it is not as striking and fresh as other features meaning it may be older than the MRE. Offset ridge of erodible and chewed up bedrock dikes within a larger saddle feature that includes channels on either side which lead to larger drainages. The piercing points and colored lines represent the displaced apex of the ridge which were roughly estimated by pacing out the distance. A large uncertainty is given based on the rough method of estimation even though the ridge crest is quite narrow.</p> <p>* - not included in slip distribution or COPD (occurs on uncertain trace).</p> <p>Note: A second fault strand without measurable offset is ~6 m to the ENE and evidenced by several small knobs, saddles, and linear features to the north and south</p>
Age interpretation	Most recent event with speculation



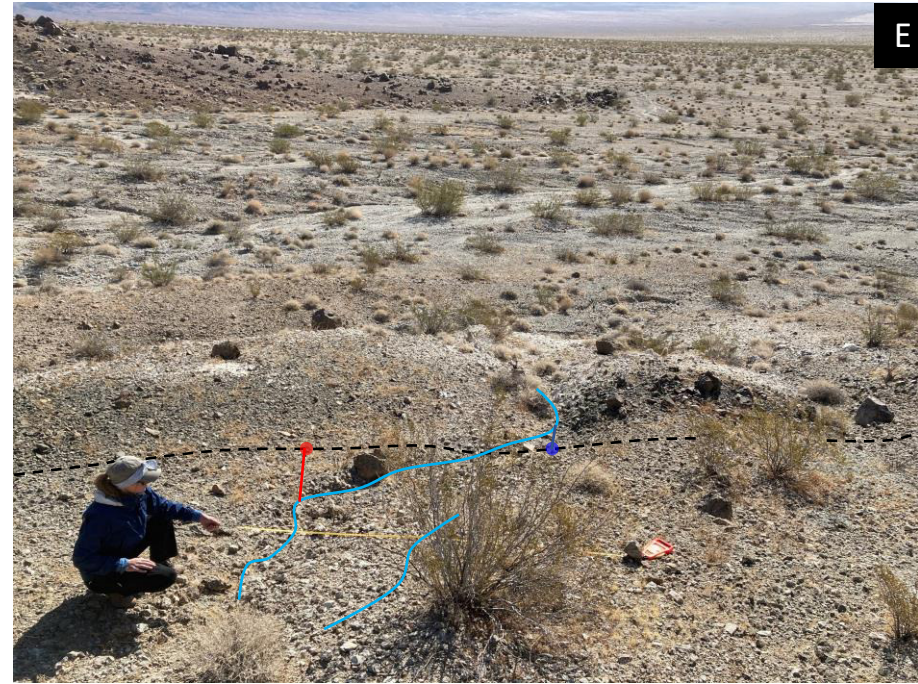
C12c

SE



## C13\*

Coordinates (Lat Lon)	34.493099°, -116.353441°
Horizontal Dextral Offset (m)	2.80 ± 0.50 m (thalweg)
Method of Measurement	Tape measure
Site Description and Uncertainty*	A higher degree of speculation is given to this offset as it is not as striking and fresh as other features meaning it may be older than the MRE. Deflected drainage incised through small fault-parallel ridge (8 m long) of fractured mafic and felsic dike forming a saddle. It is unclear if the saddle is due to the formation of a pressure ridge or if lithologically controlled. The uncertainty is based on the micro-sinuosity of the narrow channel * - not included in slip distribution or COPD (occurs on uncertain trace)
Age interpretation	Most recent event with speculation



C13b



C13a



## C14

Coordinates (Lat Lon)	34.481643°, -116.342166°
Horizontal Dextral Offset (m)	2.30 ± 0.50 m (upper riser margin)
Method of Measurement	Tape measure
Site Description and Uncertainty	Offset sited along top of irregularly defined riser. The east side is projected to fault trace (red dashed line) where eroded out by adjacent channel. The uncertainty is based on the indistinct riser margin.
Age interpretation	Most recent event



C14a

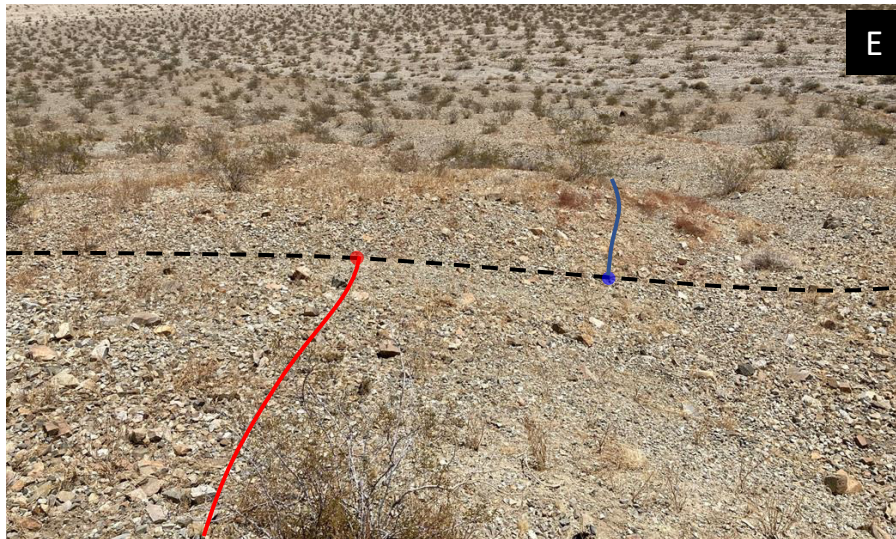


C14b



## C15

Coordinates (Lat Lon)	34.4806257°, -116.3409733°
Horizontal Dextral Offset (m)	1.70 ± 1.00 m (average)  1.20 ± 0.50 m (riser margin) 2.20 ± 0.50 m (North edge of channel)
Method of Measurement	Tape measure
Site Description and Uncertainty	A small shutter ridge and offset of an irregularly defined riser that corresponds to a displaced channel edge. An uncertainty on the average offset is assigned based on the min and max errors given for the measured features.
Age interpretation	Most recent event



C15a



C15b



## C16

Coordinates (Lat Lon)	34.480496°, -116.340910°
Horizontal Dextral Offset (m)	3.10 ± 1.20 m (upper riser margin)
Method of Measurement	Tape measure
Site Description and Uncertainty	Small shutter ridge of irregularly defined riser adjacent to broad based channel. The uncertainty was assigned with ±0.7 m on the NNW (red) piercing point and ±0.5 m on the SSE (blue) piercing point.
Age interpretation	Most recent event



C16b



C16a



C16c

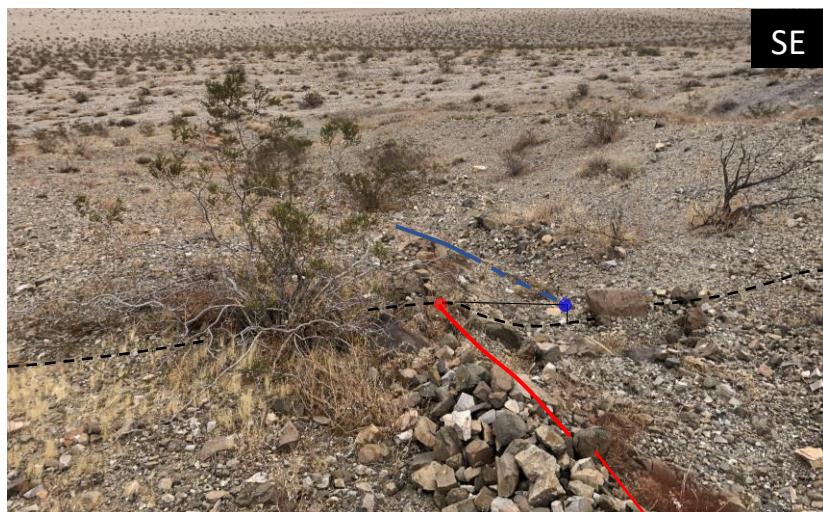


## C17

Coordinates (Lat Lon)	34.480392°, -116.340825°
Horizontal Dextral Offset (m)	2.30 ± 0.40 m (channel levee)
Method of Measurement	Tape measure
Site Description and Uncertainty	A deflected channel with most measurable section of the offset feature defined by the north edge levee of cobble sized rocks. Piercing points and colored lines follow the inside edge of the levee, and the dashed blue line represents a projection of the eroded portion of the levee edge on the east side of the fault. An uncertainty is assigned mainly due to the less defined and eroded portion of the levee.
Age interpretation	Most recent event



C17b

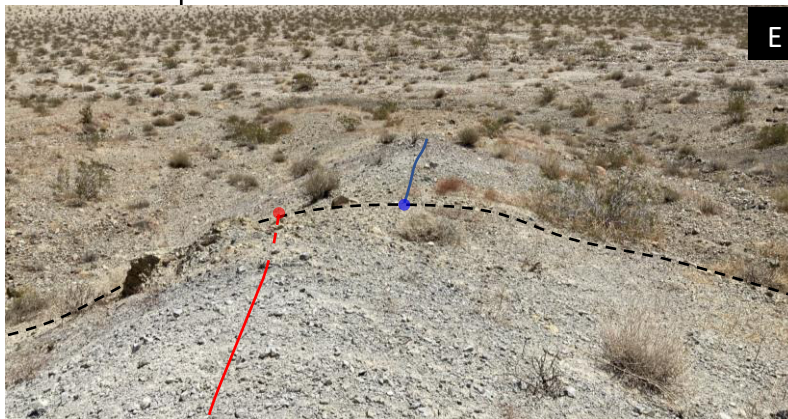


C17a

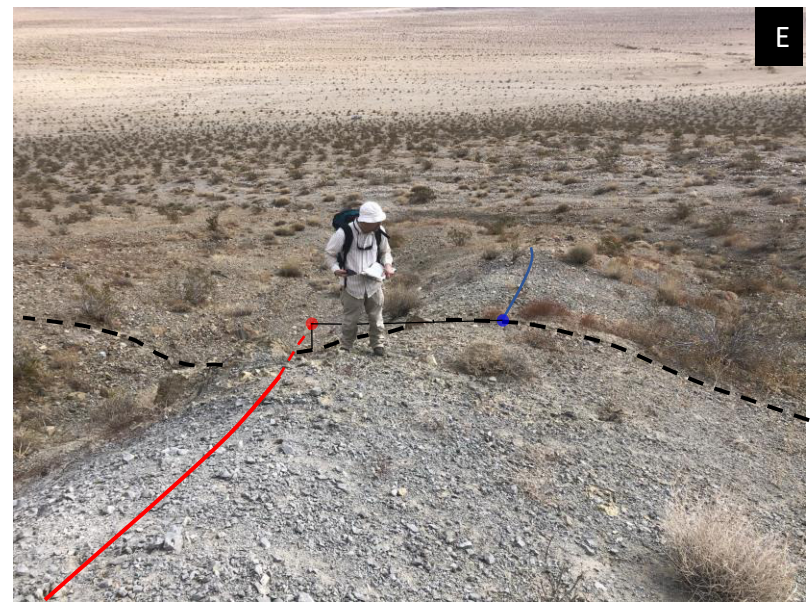


## C18

Coordinates (Lat Lon)	34.480183°, -116.340681°
Offset (m)	<u>Horizontal Dextral</u> : $2.45 \pm 0.50$ m (apex of spur ridge)  <u>Vertical</u> : $0.50 \pm 0.10$ m (west side up)  <u>Total oblique</u> : $2.50 \pm 0.60$ m
Method of Measurement	Tape measure
Site Description and Uncertainty	Offset spur ridge with gullying leading to incised channels on the north and south. The spur ridge is made up of of variably weathered and fractured leucogranite bedrock. The uncertainty is assigned because the apex is of the spur is less sharp on the east side of the fault and a projection of the piercing point from the west side of the fault was required due to erosion and a possible coseismic $\sim 0.5$ m vertical step
Age interpretation	Most recent event



C18a



C18b

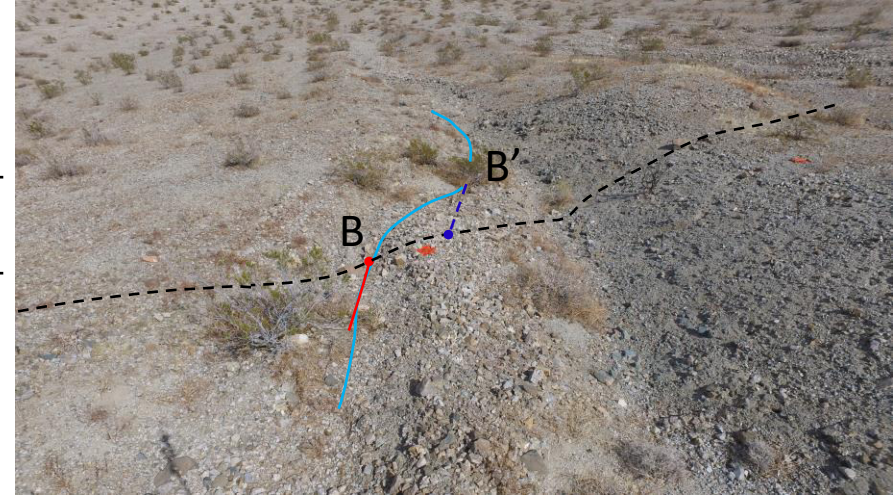


C18c

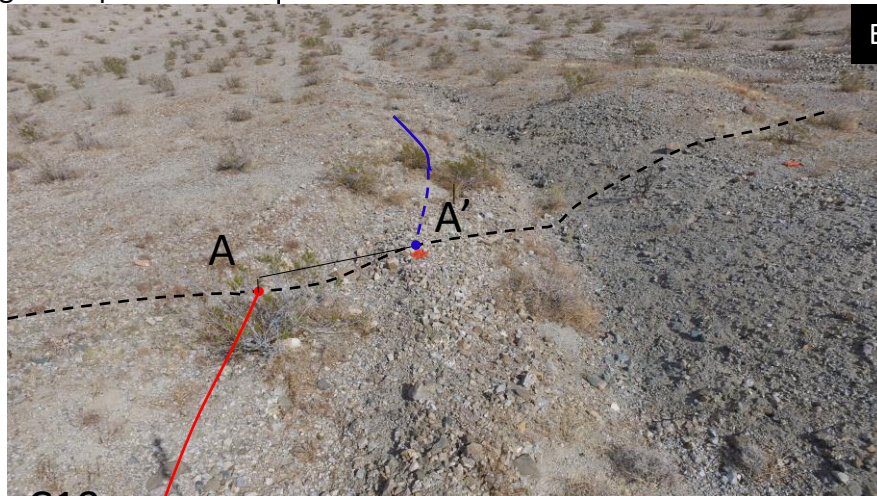


## C19

Coordinates (Lat Lon)	34.478925°, -116.339438°
Horizontal Dextral Offset (m)	3.00 ± 1.50 m (average)  A-A') 4.40 ± 0.50 m (north offset riser margin) B-B') 2.25 ± 0.60 m (north thalweg) C-C') 2.30 ± 0.60 m (south thalweg) SfM derived
Method of Measurement	Tape measure and Structure-from-Motion DEM
Site Description and Uncertainty	Clear evidence for faulting and recent rupture is defined by a narrow zone of flat disturbance that breaks the piedmont slope and has offset the drainage edges and channels. The uncertainty is based on the surface roughness and offset variability of the features in this small area. SfM hillshade and slope map assist in defining the geomorphology.
Age interpretation	Most recent event



C19b

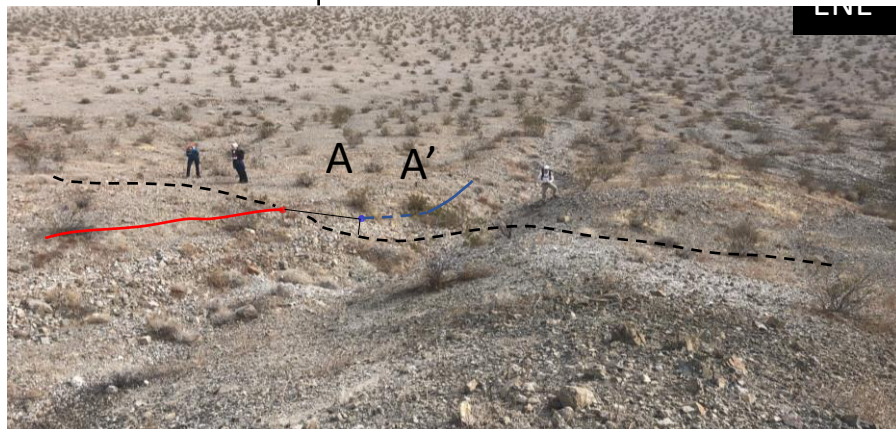
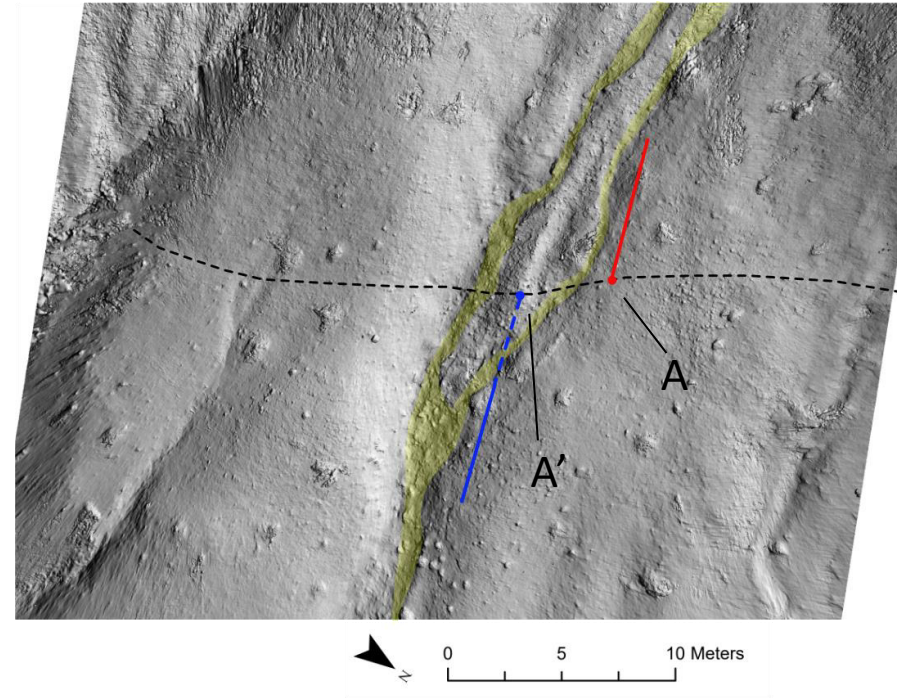


C19a



## C19

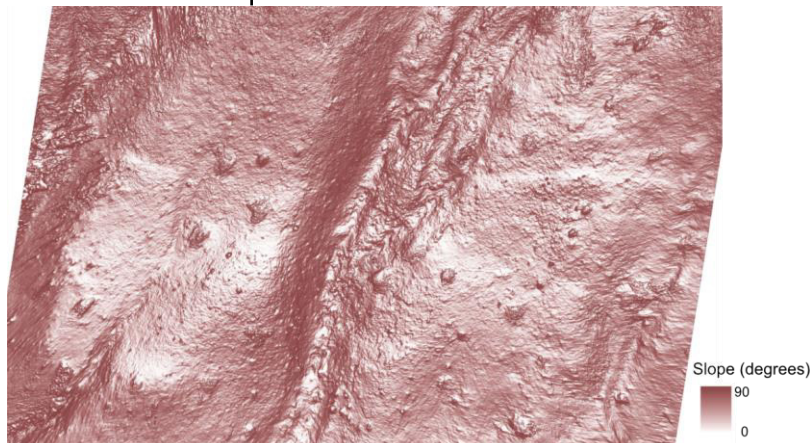
Coordinates (Lat Lon)	34.478925°, -116.339438°
Horizontal Dextral Offset (m)	3.00 ± 1.50 m (average)  A-A') 4.40 ± 0.50 m (north offset riser margin) B-B') 2.25 ± 0.60 m (north thalweg) C-C') 2.30 ± 0.60 m (south thalweg) SfM derived
Method of Measurement	Tape measure and Structure-from-Motion DEM
Site Description and Uncertainty	Clear evidence for faulting and recent rupture is defined by a narrow zone of flat disturbance that breaks the piedmont slope and has offset the drainage edges and channels. The uncertainty is based on the surface roughness and offset variability of the features in this small area. SfM hillshade and slope map assist in defining the geomorphology.
Age interpretation	Most recent event



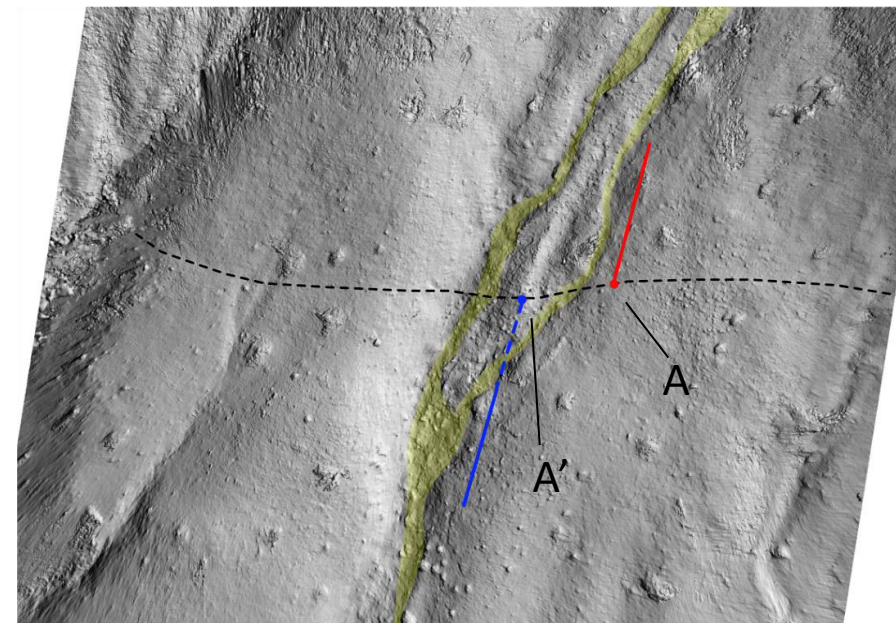


# C19

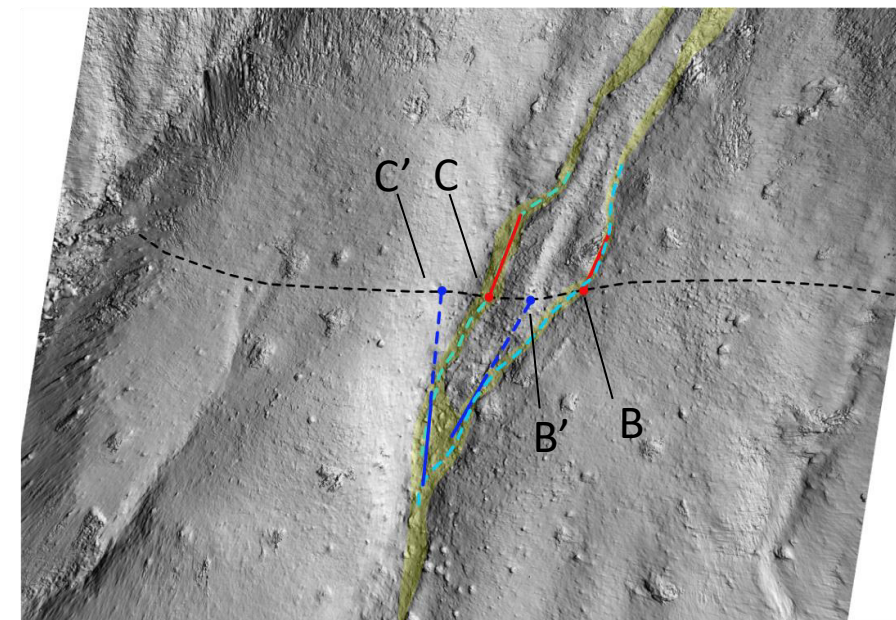
Coordinates (Lat Lon)	34.478925°, -116.339438°
Horizontal Dextral Offset (m)	3.00 ± 1.50 m (average)  A-A') 4.40 ± 0.50 m (north offset riser margin) B-B') 2.25 ± 0.60 m (north thalweg) C-C') 2.30 ± 0.60 m (south thalweg) SfM derived
Method of Measurement	Tape measure and Structure-from-Motion DEM
Site Description and Uncertainty	Clear evidence for faulting and recent rupture is defined by a narrow zone of flat disturbance that breaks the piedmont slope and has offset the drainage edges and channels. The uncertainty is based on the surface roughness and offset variability of the features in this small area. SfM hillshade and slope map assist in defining the geomorphology.
Age interpretation	Most recent event



C19e: SfM slope map



C19f: SfM hillshade  
showing A-A'

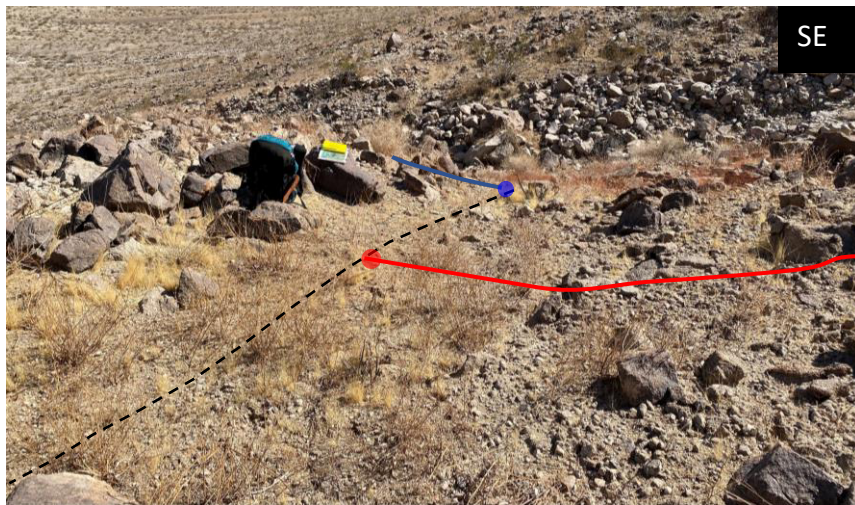


C19g: SfM hillshade showing B-B' & C-C'

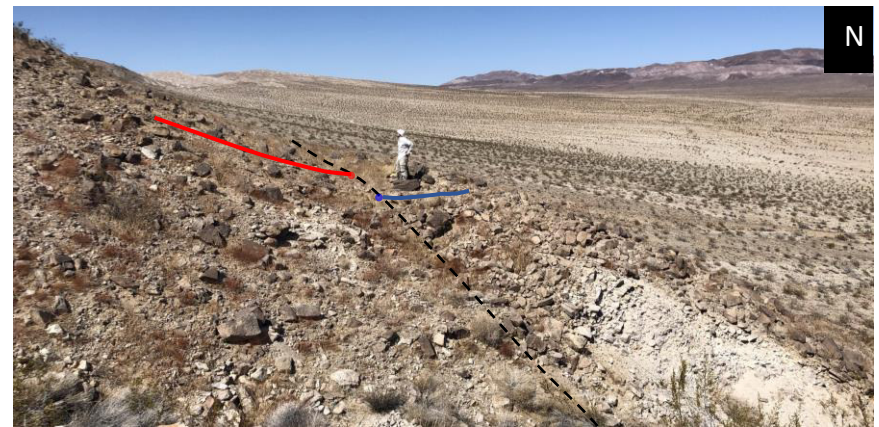


## C20

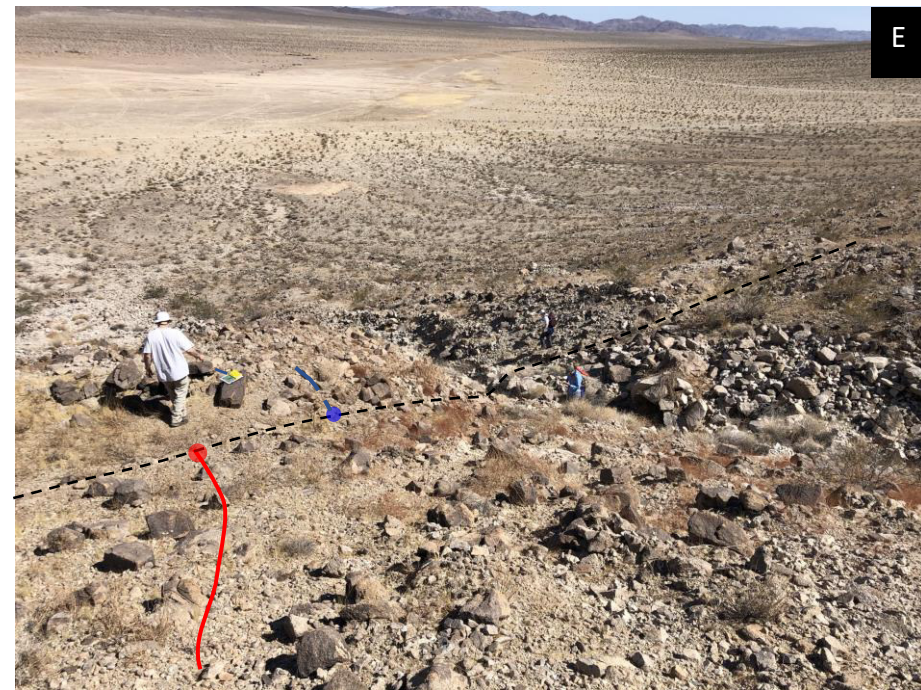
Coordinates (Lat Lon)	34.475194°, -116.336493°
Horizontal Dextral Offset (m)	2.10 ± 0.70 m (shutter panel)
Method of Measurement	Tape measure
Site Description and Uncertainty	A 2-meter-wide break in slope with grass and fines defines the location of the fault and the margin of upper drainage surface demarks the offset shutter and location of the piercing points. The margin is subtle, gradual, and a bit irregular on both sides of the fault, therefore requiring some offset uncertainty.
Age interpretation	Most recent event



C20a



C20b

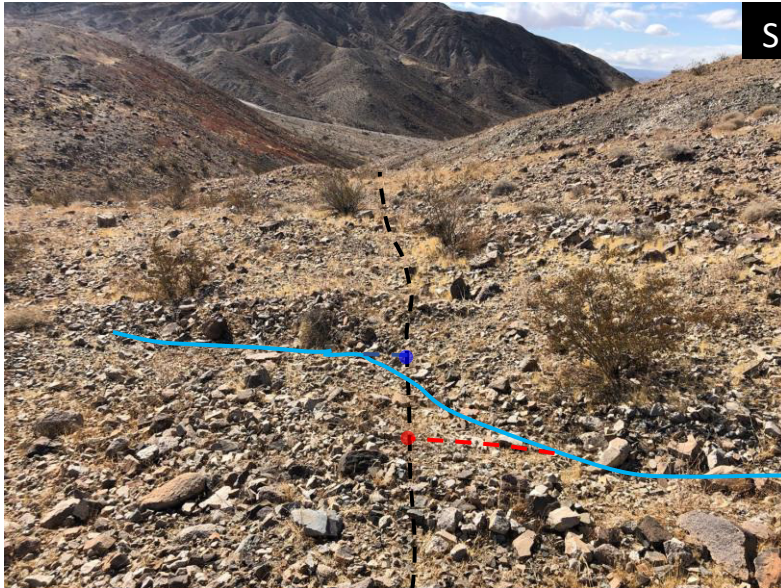


C20c



## C21

Coordinates (Lat Lon)	34.473459°, -116.335263°
Horizontal Dextral Offset (m)	1.40 ± 0.30 m (deflected channel)
Method of Measurement	Tape measure
Site Description and Uncertainty	Small deflected channel with piercing points projected to the fault from the channel thalweg. The uncertainty was assigned mostly due to the natural (not fault related) curvature of the small channel.
Age interpretation	Most recent event



C21a



C21b

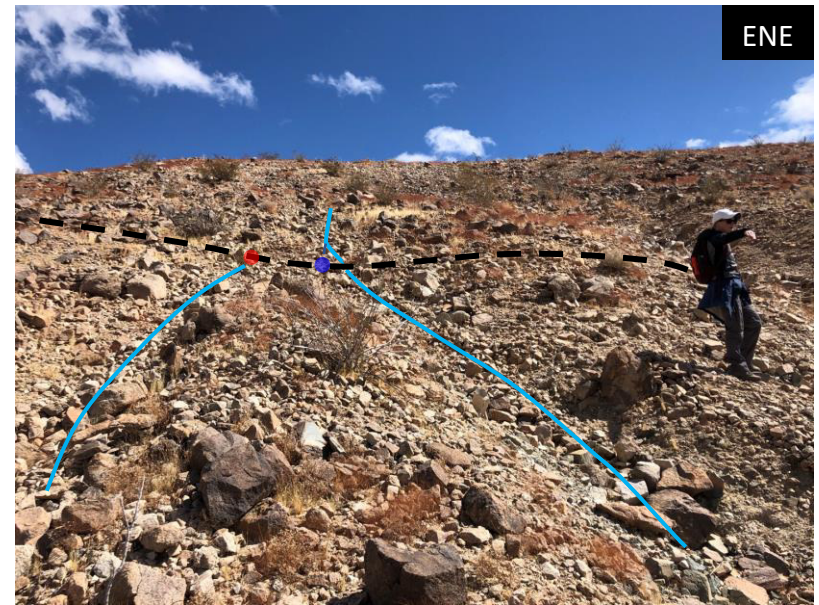


## C22#

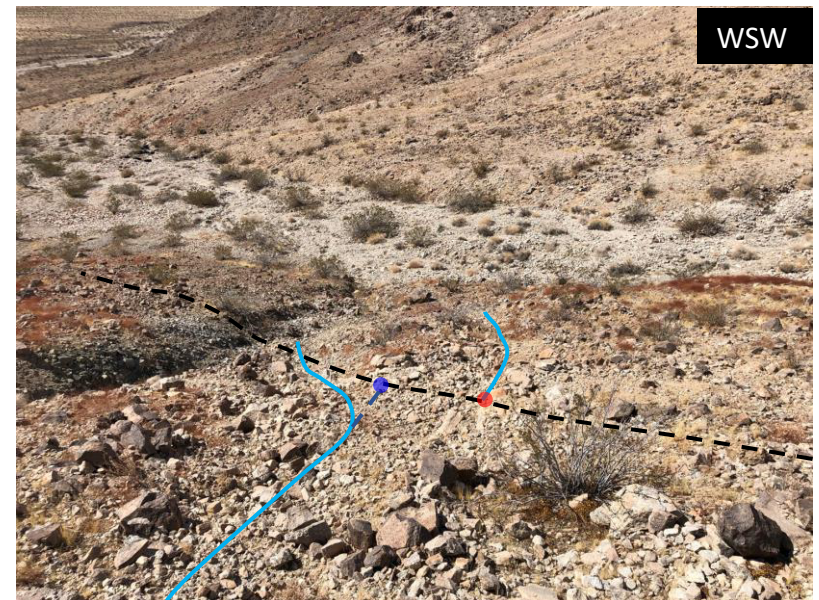
Lat Lon	34.471918°, -116.334293°
Horizontal Dextral Offset (m)	1.20 ± 0.80 m (beheaded channel)
Method of Measurement	Tape measure
Site Description and Uncertainty*	A higher degree of speculation is given to this offset as it is not as striking and fresh as other features meaning it may be older than the MRE. The offset site is on a very steep rubbly slope where the fault is defined by a continual slight break in slope that corresponds to irregularities in channels and drainages. The offset is a small beheaded and abandoned channel on the west side of the fault separated by a troughed gully of finer sediments that deflects the upslope channel to the south. # – included in COPD and slip distribution, but low level of confidence in accuracy
Age Interpretation	Most recent event with speculation



C22a



C22b



C22c



## C23#

Coordinates (Lat Lon)	34.471143°, -116.334161°
Horizontal Dextral Offset (m)	0.70 ± 0.20 m (deflected channel)
Method of Measurement	Tape measure
Site Description and Uncertainty*	A higher degree of speculation is given to this offset as it is not as striking and fresh as other features meaning it may be older than the MRE. Offset channel with piercing points projected from the thalweg. A relatively small offset error bar is due to the narrowness of the channel and certainty of fault placement. # – included in COPD and slip distribution, but low level of confidence in accuracy
Age interpretation	Most recent event with speculation



C23a



## C24#

Coordinates (Lat Lon)	34.470881°, -116.333853°
Horizontal Dextral Offset (m)	2.35 ± 1.20 m (drainage edge)
Method of Measurement	Tape measure
Site Description and Uncertainty*	<p>A higher degree of speculation is given to this offset as it is not as striking and fresh as other features meaning it may be older than the MRE. Offset drainage edge with piercing points and colored lines marking the base margins of the northern drainage edge. A large uncertainty is given due to the roughness of the surface and the presence of a smaller channel that has incised the inside edge of the ENE side of the fault leaving a colluvium peninsula.</p> <p>The smaller channel incision matches the strike of the WSW drainage margin suggesting it may be an older offset which has allowed enough time for erosion of the exposed fault plane.</p> <p># – included in COPD and slip distribution, but low level of confidence in accuracy</p>
Age interpretation	Most recent event with speculation



C24b



C24a



## C25#

Coordinates (Lat Lon)	34.470603°, -116.333611°
Horizontal Dextral Offset (m)	2.30 ± 0.70 m (drainage edge)
Method of Measurement	Tape measure
Site Description and Uncertainty*	<p>A higher degree of speculation is given to this offset as it is not as striking and fresh as other features meaning it may be older than the MRE. Offset drainage edge with piercing points and colored lines marking the base margins of the northern drainage edge. The given offset uncertainty is based on the blurry boundary between loose sloughed colluvium and intact drainage wall.</p> <p># – included in COPD and slip distribution, but low level of confidence in accuracy</p>
Age interpretation	Most recent event



C25a



C25b



## C26

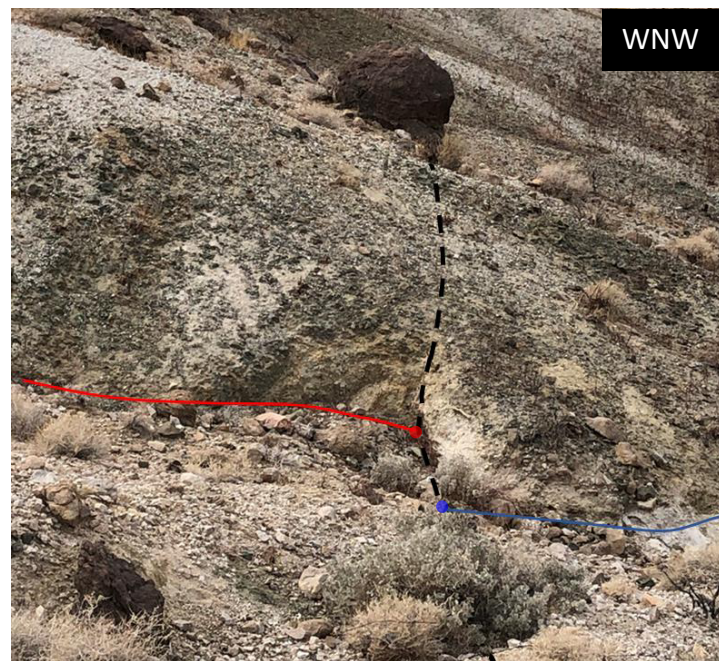
Coordinates (Lat Lon)	34.467588°, -116.329607°
Horizontal Dextral Offset (m)	1.00 ± 0.20 m (drainage edge, shutter)
Method of Measurement	Tape measure
Site Description and Uncertainty	Sharp and clean offset of pulverized mafic and felsic dike outcrop along NW drainage edge. A low uncertainty is due to the sharpness of the feature.
Age interpretation	Most recent event



C26a



C24b

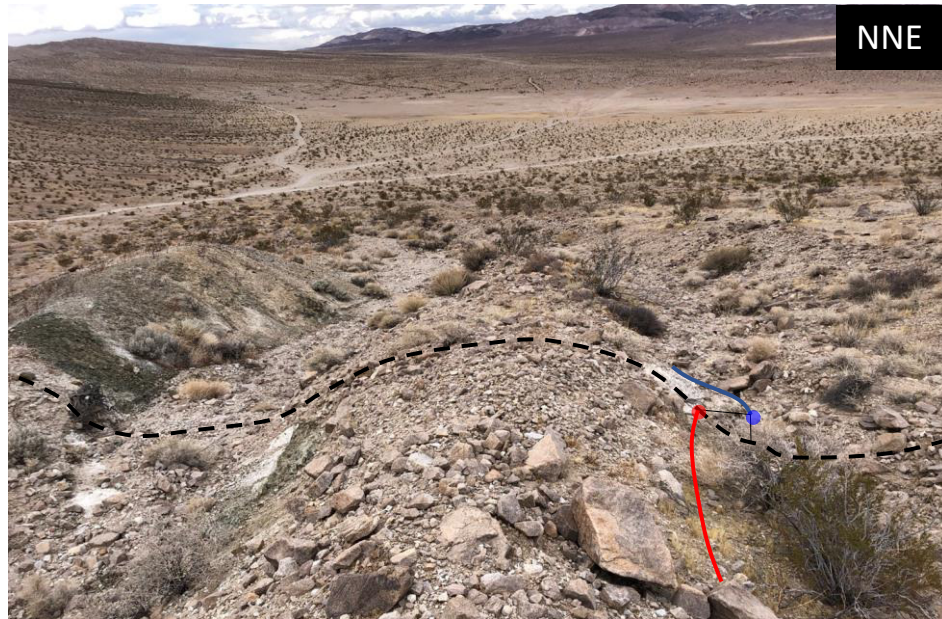


C26c



## C27

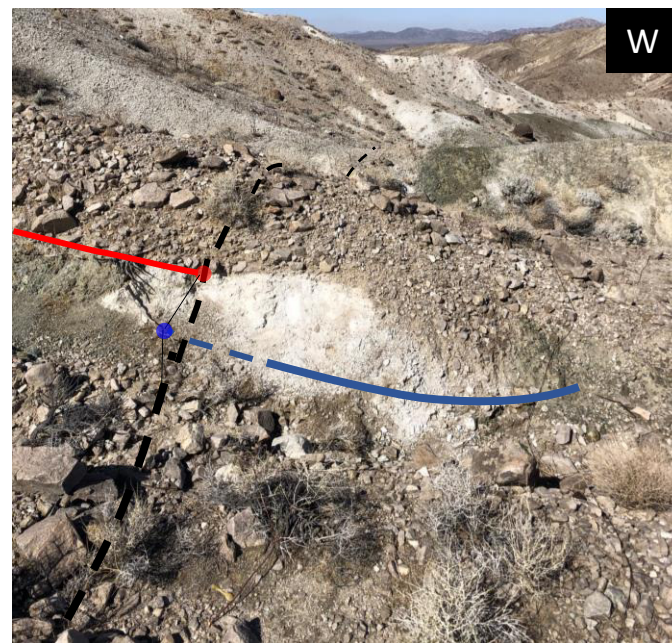
Coordinates (Lat Lon)	34.467497°, -116.329229
Horizontal Dextral Offset (m)	0.80 ± 0.30 m (drainage edge, shutter)
Method of Measurement	Tape measure
Site Description and Uncertainty	Offset spur ridge. The offset was only measured on the NNW edge of the SSE bounding drainage. Piercing points and colored lines represent the displaced basal margin of the drainage edge above the active channel. Uncertainty is due largely to the projection of the SSE margin (blue) to the fault assuming erosion.
Age interpretation	Most recent event



C27b



C27a



C27c



## C28\*

Coordinates (Lat Lon)	34.454648°, -116.307381°
Horizontal Dextral Offset (m)	1.00 ± 0.30 m (upper riser margin)
Method of Measurement	Tape measure
Site Description and Uncertainty	Small shutter panel of exposed saprolitic sheared bedrock with a thin veneer of colluvium. Piercing point and colored lines represent the upper piedmont and shutter panel margins of the adjacent SW drainage edge. The uncertainty is largely based on the projection of the shutter panel margin (blue) to the fault where we assume gullying has eroded back the fault plane. * - not included in slip distribution or COPD (occurs on uncertain trace)
Age interpretation	Most recent event



C28a



C28b



## C29\*

Coordinates (Lat Lon)	34.453167°, -116.305894°
Horizontal Dextral Offset (m)	0.70 ± 0.20 m (offset channel edge)
Method of Measurement	Tape measure
Site Description and Uncertainty	Channel edge offset of consolidated colluvium. Piercing point and colored lines represent the SE edge of a small channel. The small uncertainty was based on the relative sharpness of the channel edge. * - not included in slip distribution or COPD (occurs on uncertain trace)
Age interpretation	Most recent event



C29a



C29b



## H30

Coordinates (Lat Lon)	34.466839°, -116.335011°
Offset (m)	<p><u>Horizontal dextral</u>: <math>1.10 \pm 0.70</math> m (average)</p> <p><math>1.15 \pm 0.40</math> m (channel thalweg)</p> <p><math>1.00 \pm 0.50</math> m (NNE edge of channel)</p> <p><u>Vertical</u>: <math>0.40 \pm 0.20</math> m (South side up)</p> <p><u>Total oblique</u>: <math>1.36 \pm 0.70</math> m</p>
Method of Measurement	Tape measure
Site Description and Uncertainty	<p><u>Horizontal</u>: Deflected channel. Piercing points and colored lines of H1c represent the NNE edge of the channel while H1d shows the projected piercing points to the fault from the channel thalweg. The uncertainty was assigned to the average offset due to the shallow, subtle and lumpy nature of the channel boundaries.</p> <p><u>Vertical</u>: Irregular vertical scarp of boulder debris on the ESE side of the fault and compact finer material on the WNW side. Piercing points and lines represent the vertically displaced ground surface. The uncertainty was assigned because of the irregular boulder debris surface and projection of the upthrown surface to the fault.</p>
Age interpretation	Most recent event



H30b

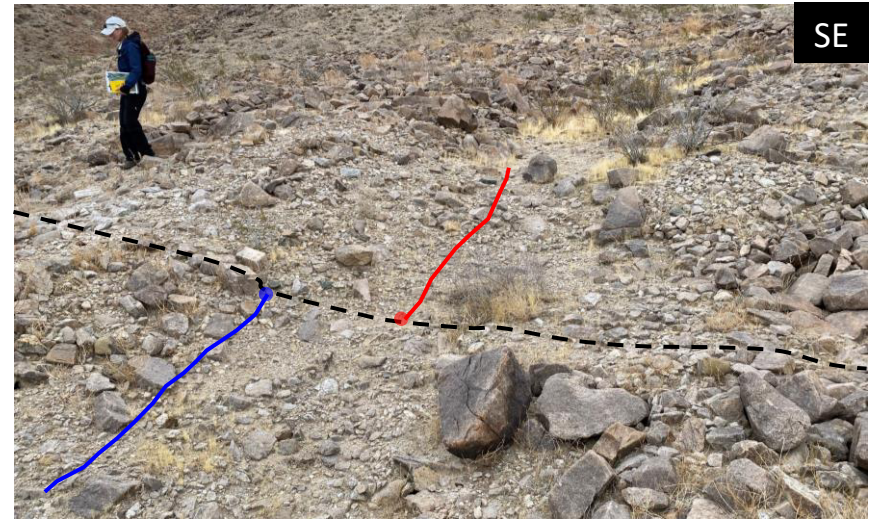


H30a



### H30

Coordinates (Lat Lon)	34.466839°, -116.335011°
Offset (m)	<p><u>Horizontal dextral</u>: <math>1.10 \pm 0.70</math> m (average)</p> <p><math>1.15 \pm 0.40</math> m (channel thalweg)</p> <p><math>1.00 \pm 0.50</math> m (NNE edge of channel)</p> <p><u>Vertical</u>: <math>0.40 \pm 0.20</math> m (South side up)</p> <p><u>Total oblique</u>: <math>1.36 \pm 0.70</math> m</p>
Method of Measurement	Tape measure
Site Description and Uncertainty	<p><u>Horizontal</u>: Deflected channel. Piercing points and colored lines of H1c represent the NNE edge of the channel while H1d shows the projected piercing points to the fault from the channel thalweg. The uncertainty was assigned to the average offset due to the shallow, subtle and lumpy nature of the channel boundaries.</p> <p><u>Vertical</u>: Irregular vertical scarp of boulder debris on the ESE side of the fault and compact finer material on the WNW side. Piercing points and lines represent the vertically displaced ground surface. The uncertainty was assigned because of the irregular boulder debris surface and projection of the upthrown surface to the fault.</p>
Age interpretation	Most recent event



H30c



H30d



## H31

Coordinates (Lat Lon)	34.464932°, -116.335994°
Horizontal Dextral Offset (m)	$1.35 \pm 0.60$ m (average)  $1.40 \pm 0.50$ m (South margin of upper drainage wall) $1.30 \pm 0.50$ m (North basal edge of drainage)
Method of Measurement	Tape measure
Site Description and Uncertainty	<p>Deflected and incised drainage with an exposed dextrally offset fault plane made up of sheared and eroded back monzonite. The piercing points and colored lines in H2a represent the basal drainage edge of the offset crushed monzonite piercing points (left pair) and margin of the upper drainage wall on the south side (right pair). The uncertainty for the average offset is based on reasonable error bars given for individual measurement on the steep and rugged channel boundaries.</p>
Age interpretation	Most recent event



H31a

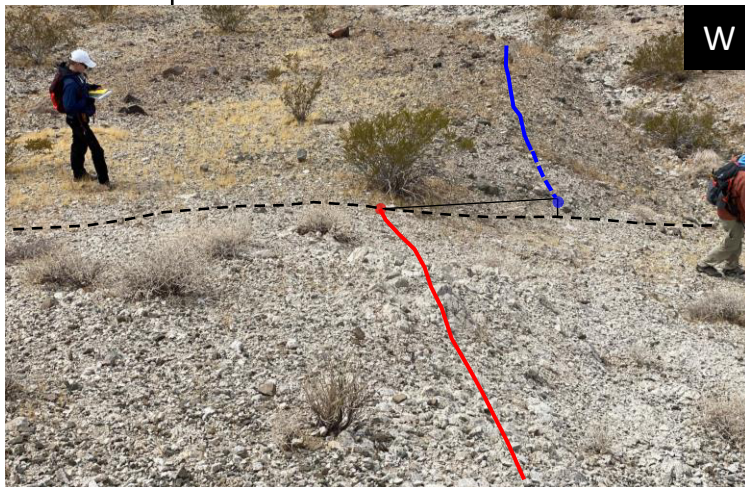


H31c



## H32

Coordinates (Lat Lon)	34.459871°, -116.336370°
Horizontal Dextral Offset (m)	1.80 ± 0.80 m (shutter panel)
Method of Measurement	Tape measure
Site Description and Uncertainty	Small shutter panel with sloughed colluvium stripped and eroded away on the east side of the fault due to gullying, exposing sheared monzonite. The piercing points and colored lines represent the displaced riser margin atop the south drainage wall. Both piercing points could be shifted north or south due to the slight irregularities of the drainage margin and difference in surface material on either side of the fault.
Age interpretation	Most recent event



H32a



H32b

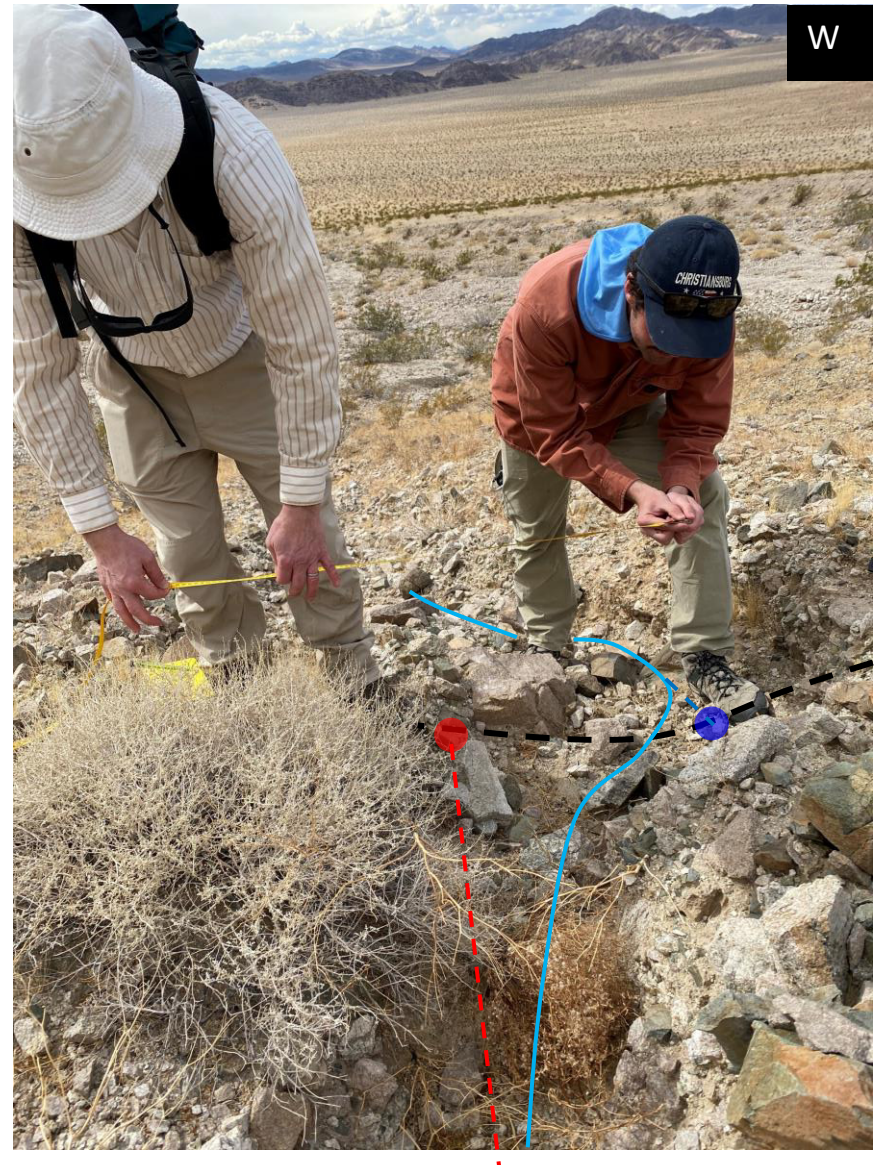


### H33

Coordinates (Lat Lon)	34.459657°, -116.336336°
Horizontal Dextral Offset (m)	0.95 ± 0.25 m (deflected channel)
Method of Measurement	Tape measure
Site Description and Uncertainty	Deflected channel on cobble and gravel sized debris veneer atop sheared monzonite. Piercing points were projected to fault from channel thalweg on either side of the fault. Uncertainty was assigned to the offset due largely to the widening of the channel on the west side of the fault and sinuous channel edges.
Age interpretation	Most recent event



H33a

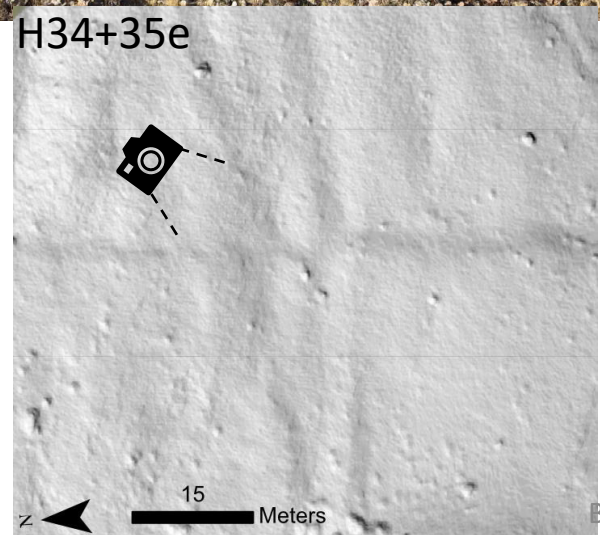
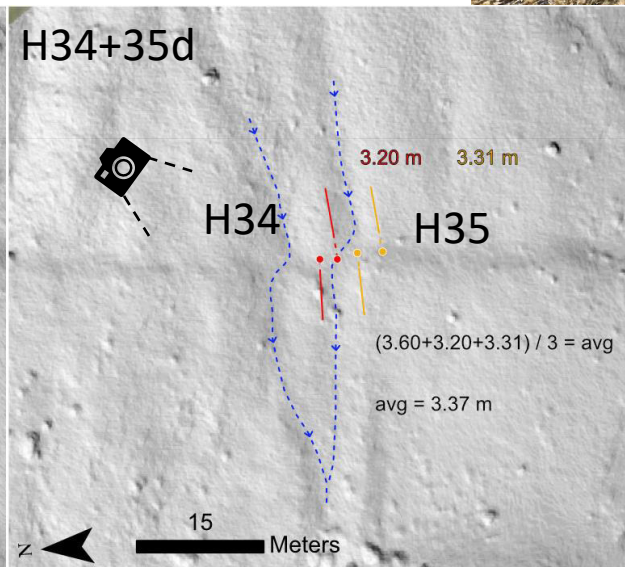
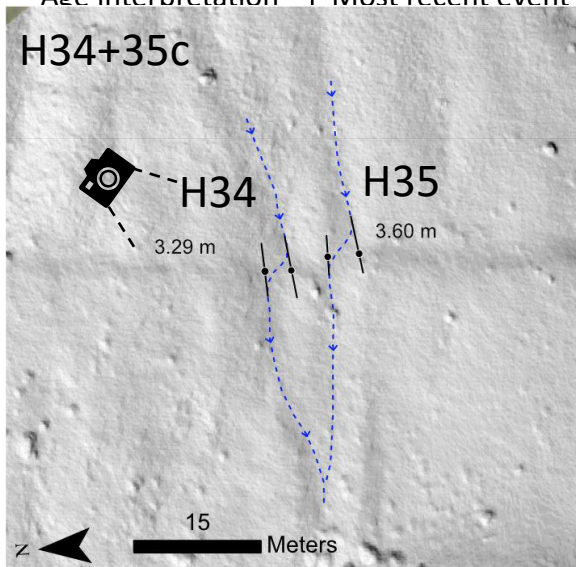
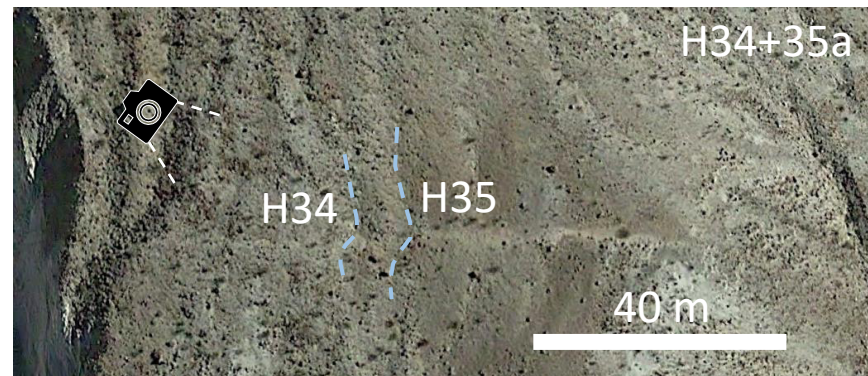


H33b



# H34"

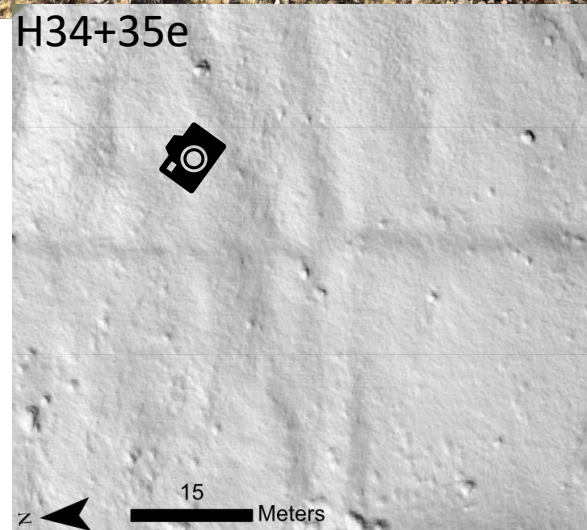
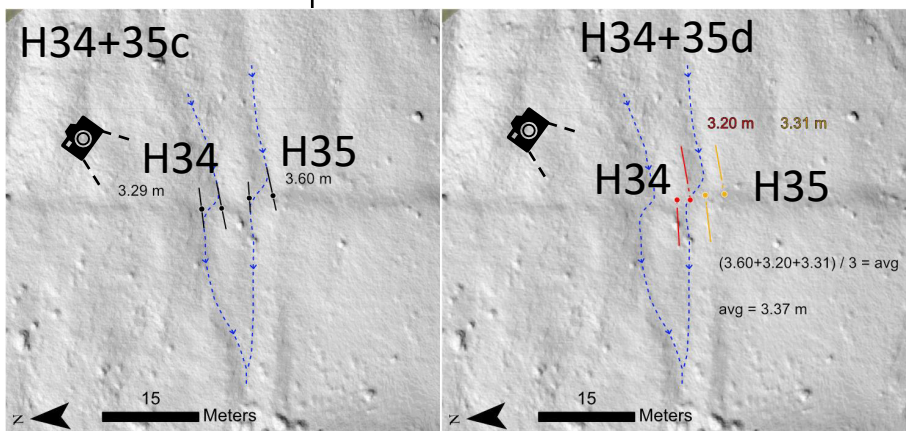
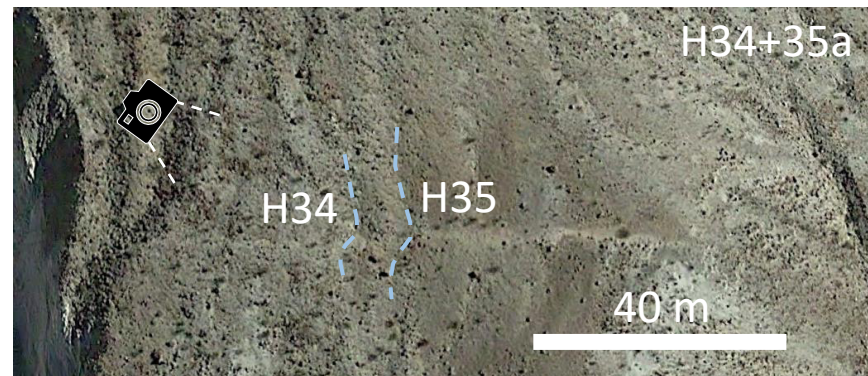
Coordinates (Lat Lon)	34.428542°, -116.316322°
Horizontal Dextral Offset (m)	3.29 ± 1.00 m (deflected channel)
Method of Measurement	" - Structure from Motion photogrammetry derived DEM measurement in GIS. Did not measure in field due to time constraints.
Site Description and Uncertainty	Deflected channel on alluvial cover along back dipping fault. Alluvium is disturbed and desert varnish is clearly broken along fault. Piercing points were projected to fault from channel thalweg on either side of the fault. Channel edges were not used because of asymmetric and poorly defined eroding morphology. Uncertainty was assigned due to no field measurement
Age interpretation	Most recent event





# H35"

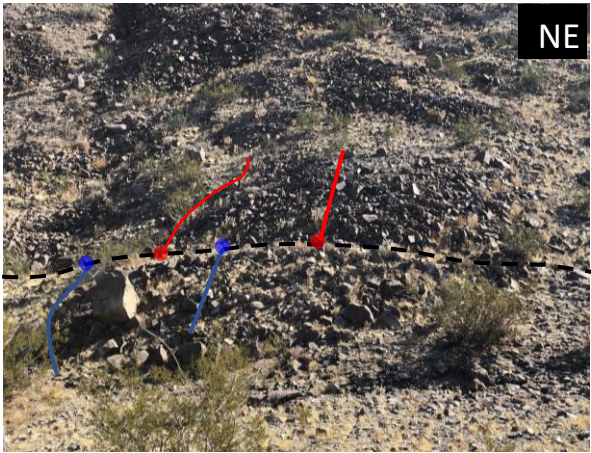
Coordinates (Lat Lon)	34.428542°, -116.316322°
Horizontal Dextral Offset (m)	$3.37 \pm 1.20$ m (average) $3.60 \pm 1.00$ m (channel thalweg) $3.20 \pm 1.00$ m (north channel boundary) $3.31 \pm 1.00$ m (south channel boundary)
Method of Measurement	" - Structure from Motion photogrammetry derived DEM measurement in GIS. Did not measure in field due to time constraints.
Site Description and Uncertainty	Deflected channel on alluvial cover along back dipping fault. Alluvium is disturbed and desert varnish is clearly broken along fault. Piercing points were projected to fault from channel thalweg on either side of the fault. Additional piercing points were projected from channel edges as they were well defined. Uncertainty was assigned due to no field measurement
Age interpretation	Most recent event



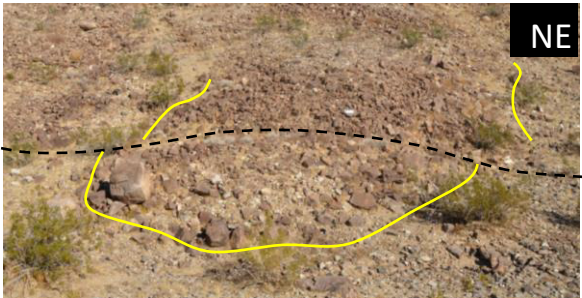


H36

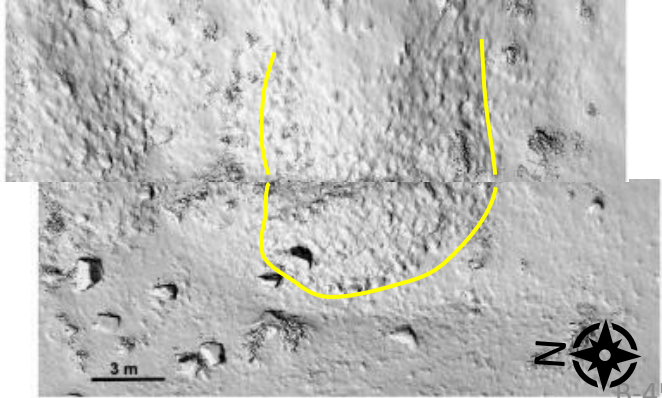
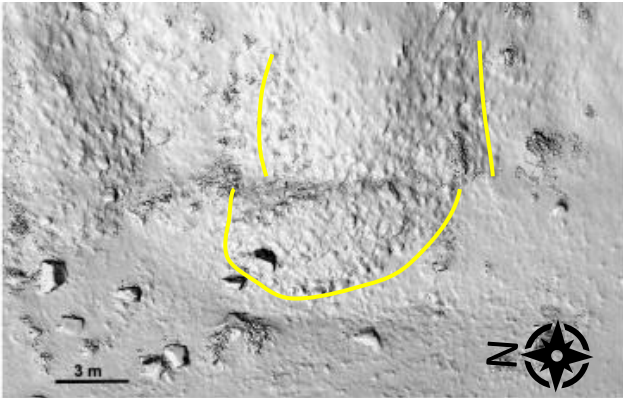
Coordinates (Lat Lon)	34.426717°, -116.315811°
Horizontal Dextral Offset (m)	1.90 ± 0.80 m (average)  1.50 ± 0.50 m (SfM DEM restoration) 2.20 ± 0.50 m (apex of boulder lobe) 2.10 ± 0.50 m (left edge of boulder lobe)
Method of Measurement	Tape measure and Structure-from-Motion DEM restoration
Site Description and Uncertainty	Offset boulder lobe at the base of a steep ridge facet. A sharp narrow continuous break in slope defines the fault and rupture location. The location of the fault was confirmed by a paleotrench dug ~20 meters south of this location. H5a shows a SfM DEM restoration and photo of the offset boulder as outlined in yellow. H6b shows the piercing points and colored lines for the field measurement of the offset north lobe edge (left pair) and the lobe apex offset (right pair). Error bars for the average offset are based on the minimum and maximum offset values for the 3 measurements taken which are largely due to the irregular lobe boundaries.
Age interpretation	Most recent event



H36b



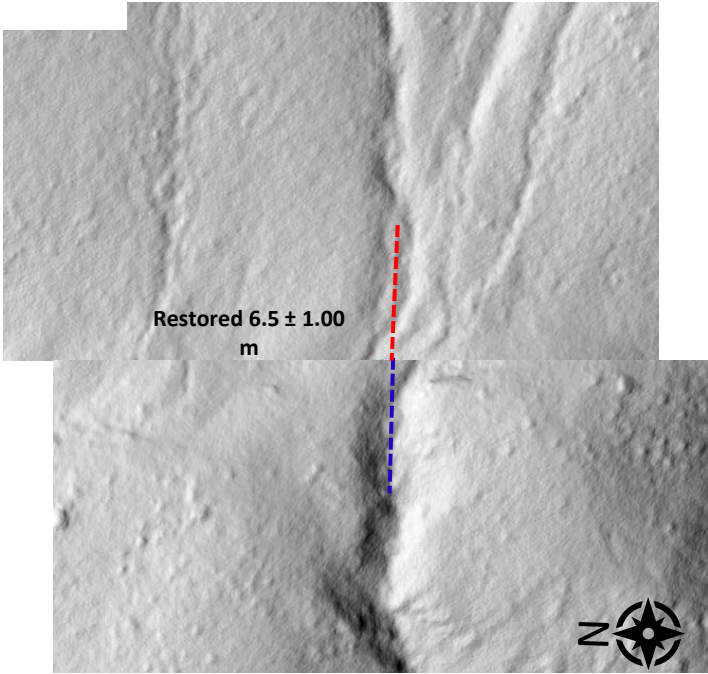
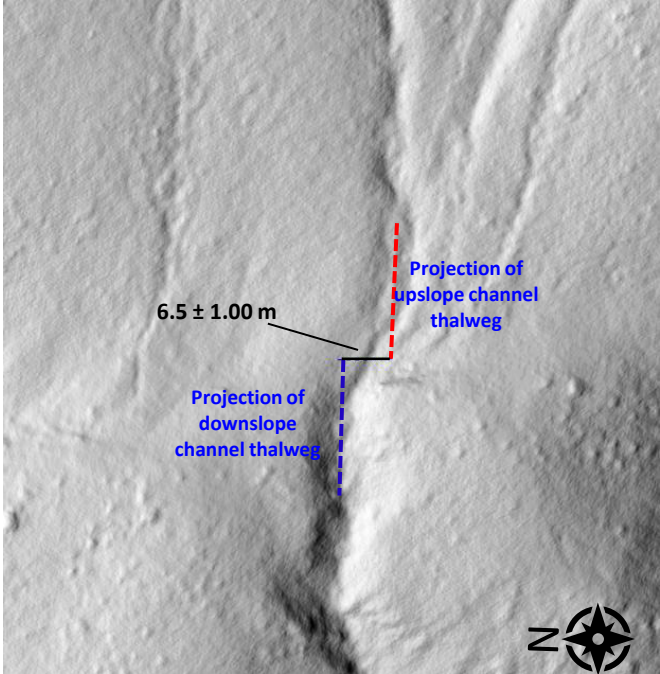
H36a





H37^”

Coordinates (Lat Lon)	34.422854°, -116.314366°
Horizontal Dextral Offset (m)	6.50 ± 1.00 m (channel thalweg)
Method of Measurement	“ - Structure-from-Motion DEM restoration
Site Description and Uncertainty	<p>The deflected channel was not measured in the field due the confluence of multiple smaller gullies and rounded eroded features making it difficult to determine piercing points. The SfM DEM more clearly defines the geomorphology of the channel.</p> <p>Uncertainties are based on difficulties defining the upslope channel projection</p> <p>^ - not included in slip distribution graph (possibly multiple events)</p>
Age interpretation	Multiple events



H37a



The shutter ridge

H38^

Coordinates (Lat Lon)	34.422436°, -116.313989°
Horizontal Dextral Offset (m)	9.40 ± 1.00 m (shutter ridge)
Method of Measurement	Electronic distance measurement (EDM)
Site Description and Uncertainty	Offset measurement piercing points were defined by the projection of the modern channel thalweg to the fault and were made in the field via EDM. Uncertainty is based on erosional widening of the channel geometry on the NE channel margin near to the fault. Though not measured in the field, a shutter ridge offset of similar magnitude is defined by the projection of the southern edge of the wash to the fault. The measured offset is clearly within a larger drainage deflection (20-25 m) indicating long term faulting of this zone, though we choose not to include the larger offset as it is not productive in addressing the topics of this study. ^ - not included in slip distribution graph (possibly multiple events)

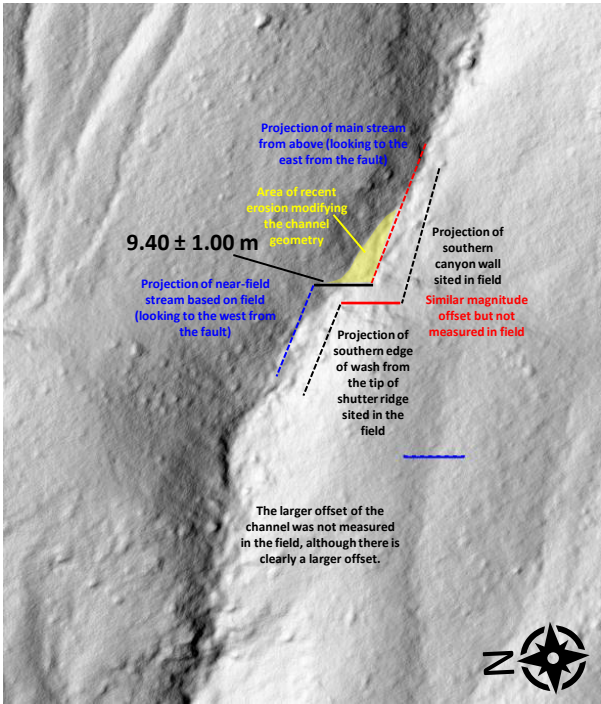
Age interpretation

Multiple events

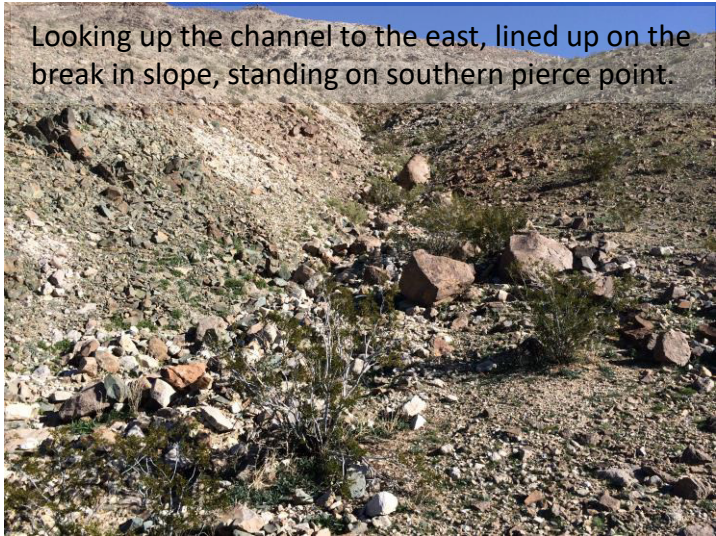
Composite photo of shutter ridge



H38a



H38b



H38c



## H38^

Coordinates (Lat Lon)	34.422436°, -116.313989°
Horizontal Dextral Offset (m)	9.40 ± 1.00 m (shutter ridge)
Method of Measurement	Electronic distance measurement (EDM)
Site Description and Uncertainty	<p>Offset measurement piercing points were defined by the projection of the modern channel thalweg to the fault and were made in the field via EDM. Uncertainty is based on erosional widening of the channel geometry on the NE channel margin near to the fault. Though not measured in the field, a shutter ridge offset of similar magnitude is defined by the projection of the southern edge of the wash to the fault. The measured offset is clearly within a larger drainage deflection (20-25 m) indicating long term faulting of this zone, though we choose not to include the larger offset as it is not productive in addressing the topics of this study.</p> <p>^ - not included in slip distribution graph (possibly multiple events)</p>

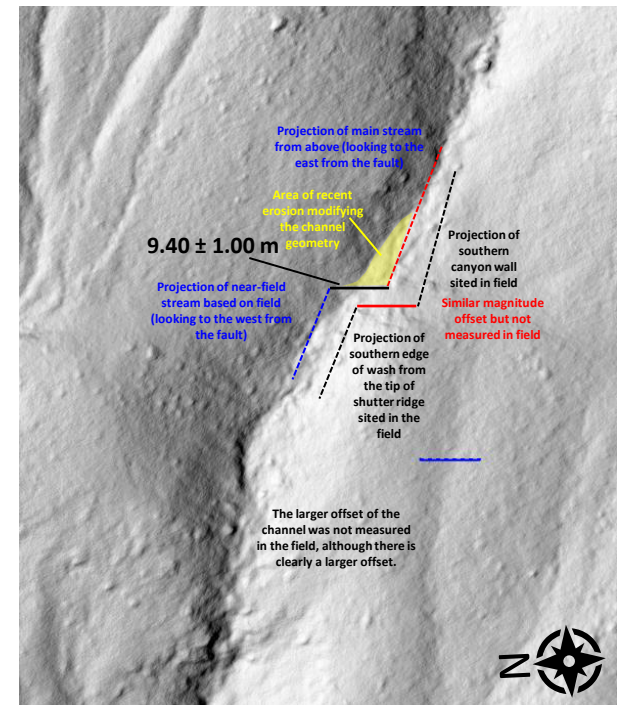
## Age interpretation

## Multiple events

Composite photo of shutter ridge

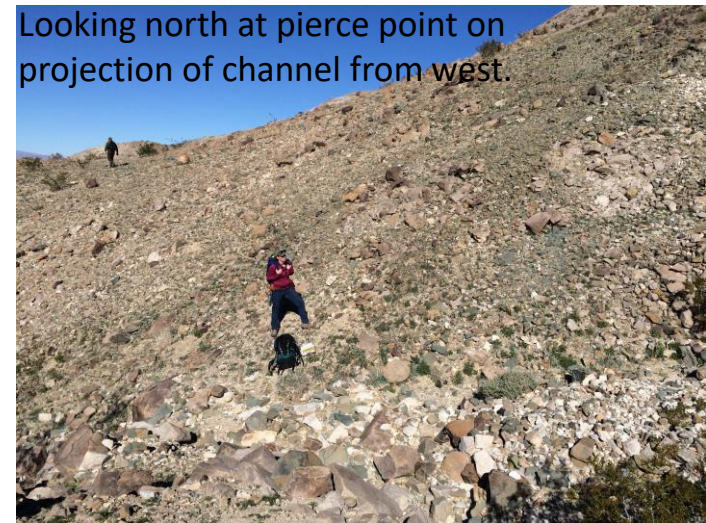


H38a



H38b

Looking north at pierce point on  
projection of channel from west.

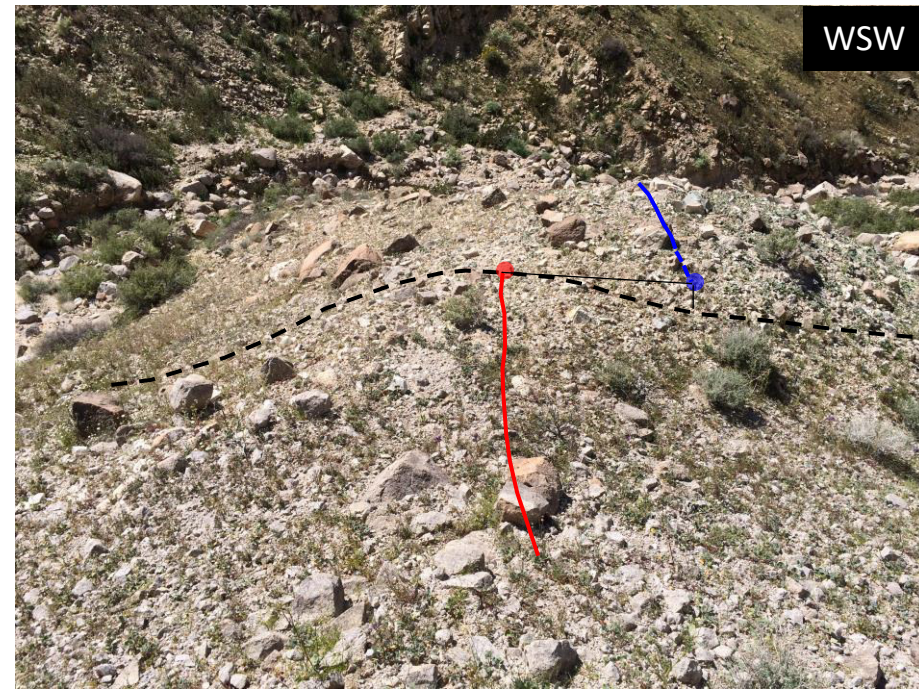


H38d

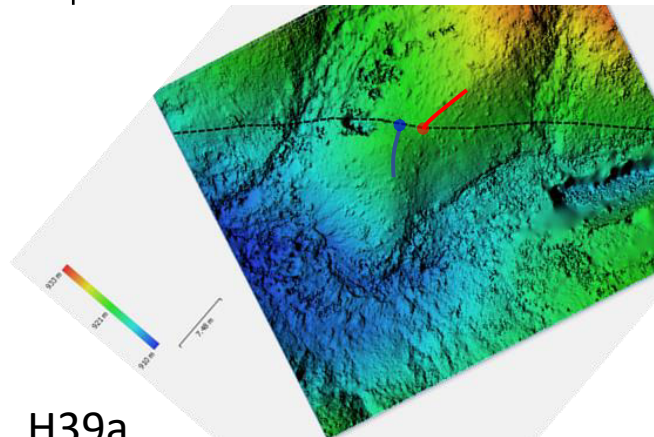


## H39

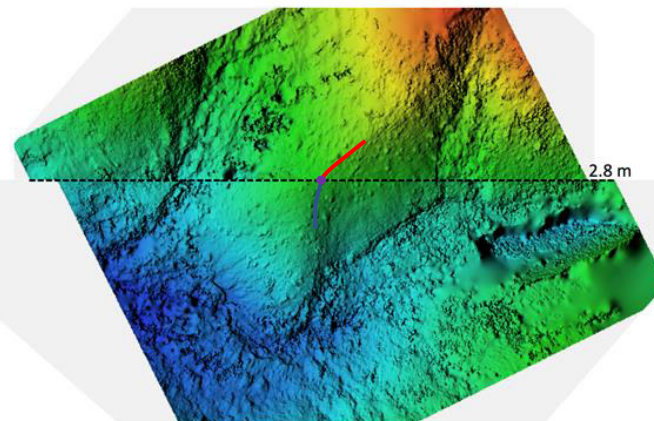
Coordinates (Lat Lon)	34.40966°, -116.29758°
Horizontal Dextral Offset (m)	3.10 ± 1.80 m (average)  3.40 m (+2.70 m, -1.30 m) (tape measure of shutter) 2.80 m ± 1.00 m (SfM DEM restoration)
Method of Measurement	Tape measure and Structure-from-Motion DEM restoration
Site Description and Uncertainty	Shutter ridge consisting of colluvium on the steep canyon wall, where the Hidalgo fault appears as a sharp linear cut with uphill-facing scarps along strike. H6a is the SfM DEM restoration of the offset and H7b is the annotate field measurement which was taken on the crest of the spur ridge. Offset uncertainty of SfM DEM and field measurements are due to the broadness and rounded nature of the crest.
Age interpretation	Most recent event



H39b



H39a





## H40

Coordinates (Lat Lon)	34.40926°, -116.29720°
Horizontal Dextral Offset (m)	4.30 ± 2.00 m (shutter ridge)
Method of Measurement	Tape measure
Site Description and Uncertainty	Colluvium shutter ridge defined by a back-facing scarp on a steep canyon wall. Hidalgo fault appears as a sharp linear and narrow zone of loose disturbance. The offset uncertainty based on the roundedness of the feature making it difficult to pinpoint margins for piercing point placement. This is likely due to the softness and erodibility of the material, which is also added evidence for the youngness of the features
Age interpretation	Most recent event



H40b

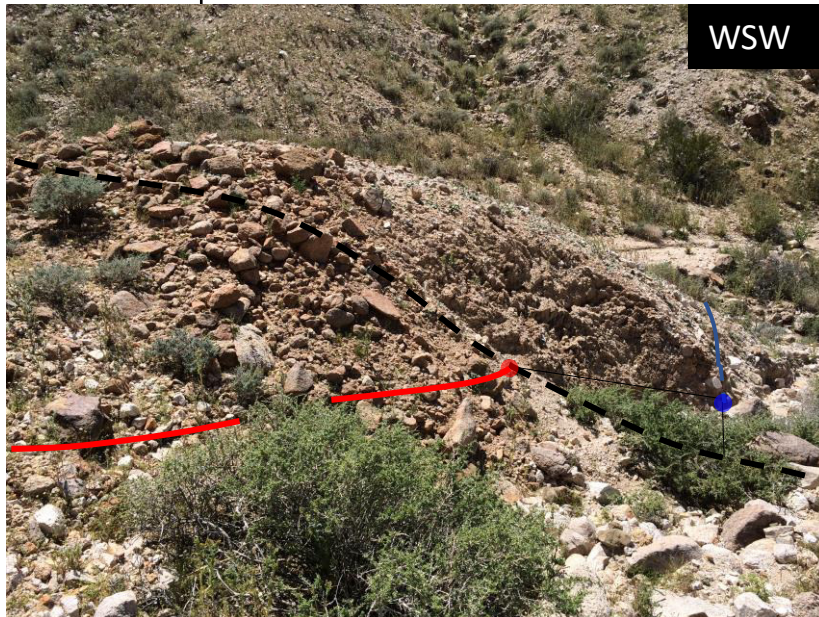


H40a

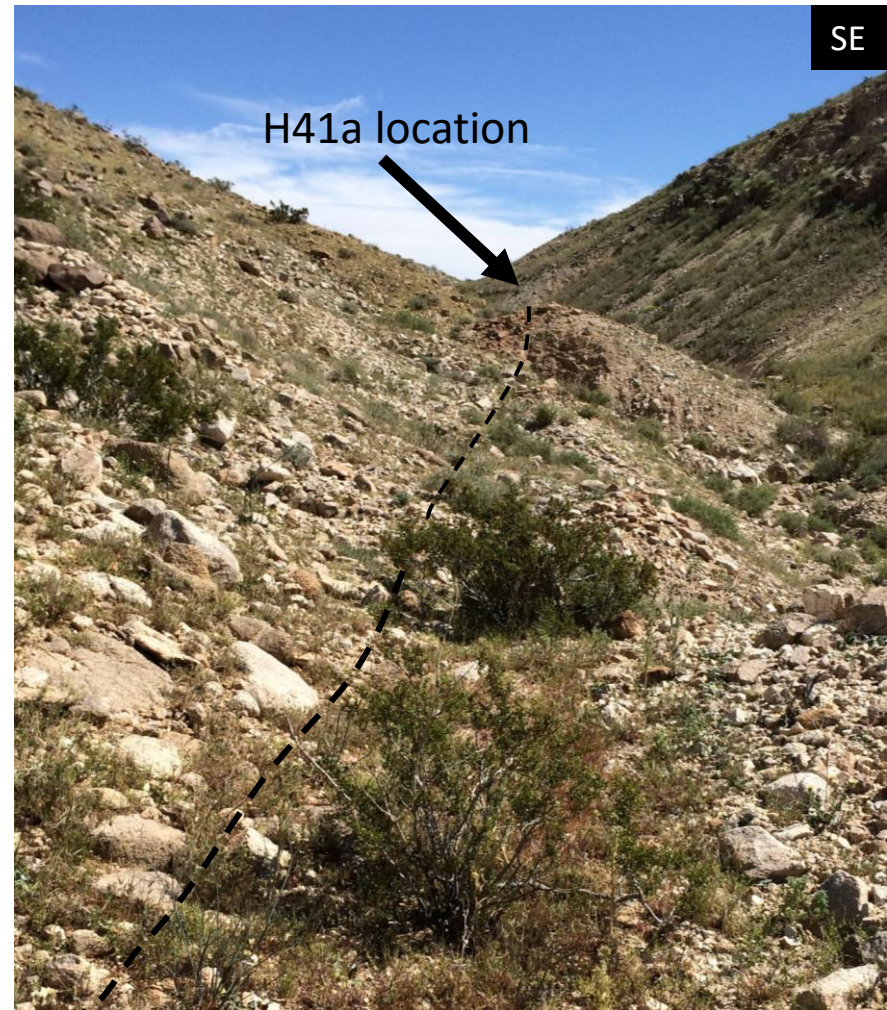


## H41"

Coordinates (Lat Lon)	34.40902°, -116.29699°
Horizontal Dextral Offset (m)	2.5 ± 1.5 m (shutter ridge)
Method of Measurement	" - By eye and the Google Earth measuring tool. Did not measure with tape due time constraints.
Site Description and Uncertainty	Shutter ridge with sharp colluvial face and trough that gullies from the break in the slope to the fault-parallel drainage. H9a show piercing points and colored lines that represent the basal edge of the displaced shutter ridge and SE drainage edge.
Age interpretation	Most recent event



H41a



H41b



## **Supplemental Material, Part C: Additional methods, results, data discussion, and references for OSL and IRSL geochronology.**

We collected eight samples for optically stimulated luminescence (OSL) and infrared stimulated luminescence (IRSL) dating from the upper sand-rich units, with four samples from trench 1 and four from trench 2. Samples were collected on the shaded (south) trench wall, with the wall surface cut back ~5 cm before driving the sample tubes into the wall. Sample tubes were sections of 1.5-inch- and 2-inch-diameter metal pipes, which were capped with plastic caps and duct tape to protect from light contamination. Samples were shipped to the Luminescence Laboratory at North Carolina State University.

OSL dating determines the time elapsed since a sediment sample was last exposed to daylight (Aitken, 1998). The method relies on the interaction of ionizing radiation with electrons in semi-conducting minerals within buried sediment, which results in metastable charge accumulation. The incidence of light or heat in the mineral grains releases the charged ions as a measurable emission of photons (luminescence). The various luminescence methods assume that mineral grains were exposed to daylight during or immediately before the transport, which will set them to their geological zero residual level. Upon burial, the daylight exposure ceases, and the luminescence signal accumulates due to the radiation arising from the decay of ambient radioisotopes that include U, Th, Rb, and K, and from cosmic rays. Given that, as a first approximation, the radiation exposure (the dose rate -  $D_R$ ) is constant over the timescales of interest, luminescence builds up (equivalent dose -  $D_E$ ) in the minerals in proportion to the duration of burial and the concentration of the radioisotopes in the sample environment and the cosmic dose. The sample's depositional age ( $A$ ) is thus a ratio of luminescence acquired and the rate of luminescence acquisition, i.e.,  $A = D_E / D_R$  (Aitken, 1998; Murray and Olley, 2002; Singhvi and Porat, 2008).

*Preparation and measurement* - All sediment samples were prepared for quartz and feldspar OSL dating under safe light conditions. The sediment from the ends of each tube was cut off, dried to determine the water content, and then crushed and sent to the Activation Laboratories Limited in Ancaster, Ontario, Canada for Major Elements Fusion ICP/MS/Trace Elements analysis to determine the U, Th, Rb, and K concentrations for  $D_R$  calculations (Table 1 in main manuscript). The  $D_R$  for each sample was calculated through the DRAC (Dose Rate and Age Calculator) online calculator from Aberystwyth University, assuming the U, Th, Rb, and K concentration, location, elevation, depth, and water content (Durcan et al., 2015).

The remaining sediment was pretreated with 10% HCl and 10% H<sub>2</sub>O<sub>2</sub> to remove carbonates and organic matter. The pretreated samples were rinsed in water, dried, and sieved to extract the 90–150  $\mu$ m particle size fraction. A sub-fraction (~20 g) of sediment was etched using 10% HF acid for 10 minutes to remove the outer alpha-irradiated layer from feldspar grains. Any fluorides precipitated during HF treatment were removed using 17% HCl for 45 min. The sample was then rinsed in distilled water.

Next, a low field-controlled Frantz isodynamic magnetic separator (LFC Model-2) was used to separate feldspar and magnetic minerals from quartz in the 90–150 $\mu$ m particle size fraction following the methods of Porat (2006) with the slope and tilt angles set to 25° and 17°,



respectively. This was followed by density separation using lithium polytungstate (LST) at densities of 2.56, 2.58, 2.62, 2.68 was used to extract K-feldspar at a density of 2.56–2.58 and quartz at a density of 2.62–2.68. The samples were then sieved to remove any grains smaller than 90  $\mu\text{m}$  and collect the 150–250  $\mu\text{m}$  fraction. The K-feldspar fraction was rinsed in distilled water and acetate, dried, and then ready for infrared stimulated luminescence (IRSL) measurements.

The quartz fraction was etched using 44% HF acid for 45 minutes to remove the outer alpha-irradiated layer from quartz particles. This treatment also helps dissolve any other silicate grains present. Any fluorides precipitated during HF treatment were removed by etching the sample in 37% HCl for 30 min. The quartz sample was then rinsed in distilled water and acetate and dried. The result for the quartz isolation was then sieved using a 90  $\mu\text{m}$  mesh to remove any grains smaller than 90  $\mu\text{m}$ , so that the 90–150  $\mu\text{m}$  could be used for blue light stimulated luminescence (BLSL).

An automated Risø OSL reader model TL-DA-20 was used for OSL measurements and irradiation. Aliquots containing several hundred grains of quartz or feldspar were mounted onto ~ 6 mm diameter stainless steel discs as a small central circle ~ 3 mm in diameter.

For quartz dating, aliquots for each sample were first checked for feldspar contamination using IRSL at room temperature before the main OSL measurements were undertaken (Jain and Singhvi, 2001). If the aliquots did not pass the IRSL test, the samples were etched in 40% HF for another 30 minutes to remove any remaining feldspar, followed by 10% HCl treatment and sieving again. Only aliquots that passed the IRSL test were used for OSL dating. Aliquots of quartz were illuminated with blue LEDs stimulating at a wavelength of 470 nm BLSL. The detection optics comprised Hoya U-340 and Schott BG-39 color glass filters coupled to an EMI 9235 QA photomultiplier tube. The single aliquot regeneration (SAR) method of Murray and Wintle (2000, 2003) was used to determine the  $D_E$  for age estimation. Only aliquots that satisfy the criterion of a cycling ratio <10% were used in determining  $D_E$ . A preheat of 240 °C for 10s was used, and the OSL signal was recorded for 40 s at 125 °C. OSL sensitivity of the samples had a high signal-to-noise ratio. For quartz, dose recovery tests (Wintle and Murray, 2006) indicate that a laboratory dose of 10.9 Gy could be recovered to within 10% by the SAR protocol suggesting that the protocol was appropriate.

For feldspar dating, aliquots of samples were illuminated with IR LEDs stimulating at an 830 nm wavelength. The detection optics comprised Hoya U-340 and Schott BG-39 color glass filters coupled to an EMI 9235 QA photomultiplier tube. The samples were irradiated using a  $^{90}\text{Sr}/^{90}\text{Y}$  beta source. The single aliquot regeneration (SAR) method of Murray and Wintle (2000; 2003) was also used to determine the  $D_E$  for age estimation for feldspar. Only aliquots that satisfy the criterion of a recycling ratio <10% were used in determining  $D_E$ . A post-IR IRSL protocol was used with a preheat of 250°C for 60s and 159 stimulation temperatures of 50°C and 225°C. IRSL sensitivity of the samples had a very high signal-to-noise ratio. The samples were tested for anomalous thermal fading (Huntley and Lamothe, 2001) for timescales ranging from ~300 seconds to 1 day. None of the samples show fading, and no correction was required.



Both quartz (BLSL) and feldspar ages were calculated assuming a weighted mean  $D_E$  and a mixing model equivalent dose (Galbraith, 1990; Galbraith and Green, 1990), and graphical plots of the equivalent dose distribution were done using Radial Plotter (Vermeesch, 2009, version 9.5). For the samples with equivalent dose dispersion larger than 20%, we applied a mixing model for 2 populations and assumed the first population peak as representative of the last burial moment. When samples have a narrow distribution despite their dispersion, the ages calculated by both methods are very similar.

The graphical plots for samples 2019OSL1, 2019OSL1, 2019OSL2, T101, T102, T203, T203, T204, T205, and T206 are presented in Figures S7–S16.

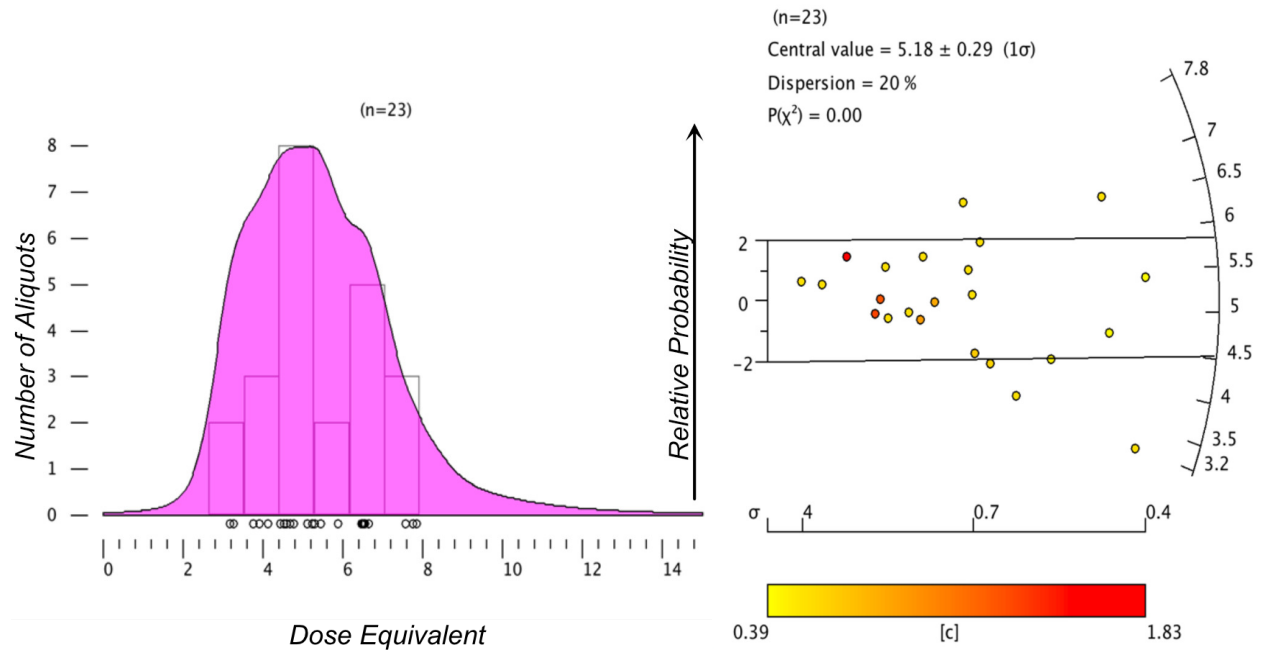


Figure S7. Relative probability histogram and radial plot for the distribution of  $D_E$  measurements in aliquots from sample '2019OSL1'. These are BLSL measurements on quartz grains, with IRSL measurements on feldspar from the same sample shown in Figure S8. Yellow to red values on the scale bar [c] indicates the uncertainty associated with individual  $D_E$  measurements. Age results are shown in Table 1 in the main manuscript.



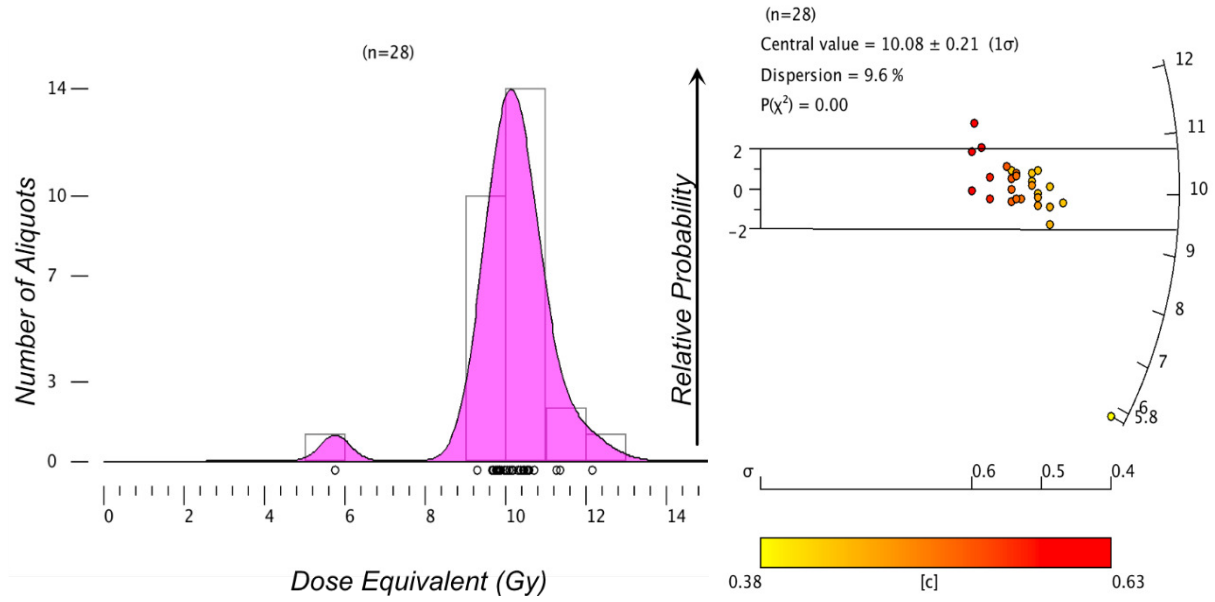


Figure S8. Relative probability histogram and radial plot for the distribution of  $D_E$  measurements in aliquots from sample '2019OSL1'. These are IRSL measurements on feldspar grains, with BSL measurements on quartz from the same sample shown in Figure S7. Yellow to red values on the scale bar [c] indicates associated uncertainty for individual  $D_E$  measurements. Age results are shown in Table 1 in the main manuscript.

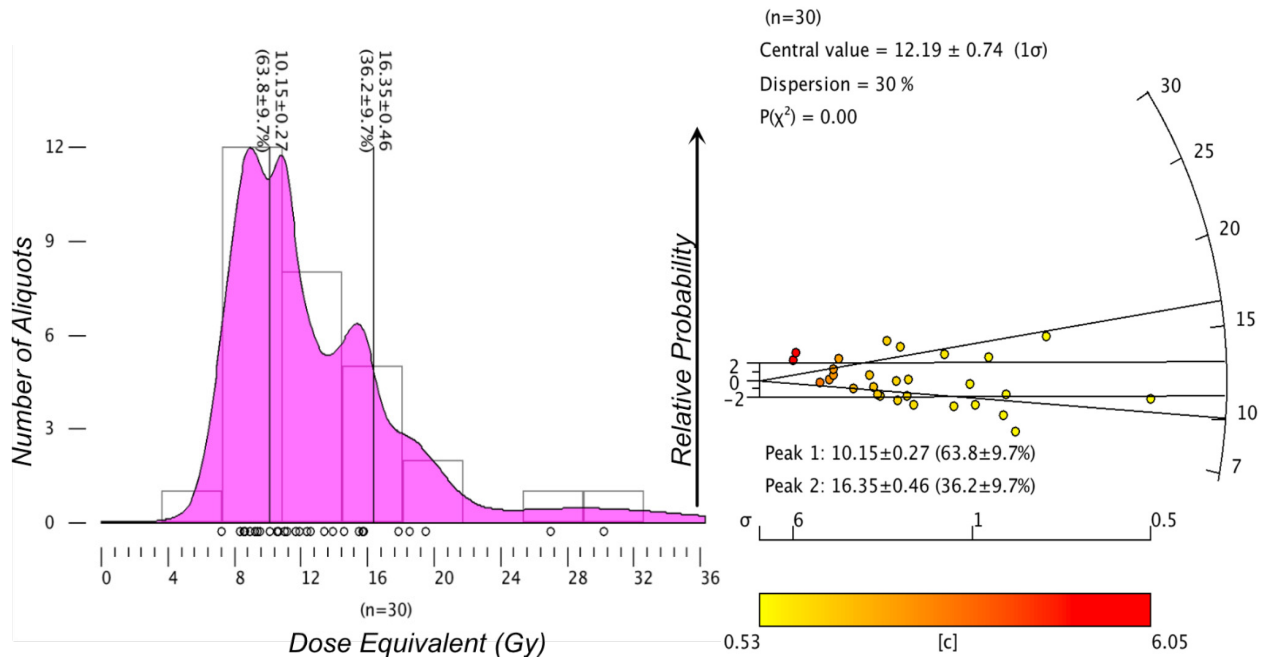


Figure S9. Relative probability histogram and radial plot for the distribution of  $D_E$  measurements in aliquots from sample '2019OSL2'. These are BSL measurements on quartz grains. Yellow to red values on the scale bar [c] indicates associated uncertainty for individual  $D_E$  measurements. Age results are shown in Table 1 in the main manuscript.



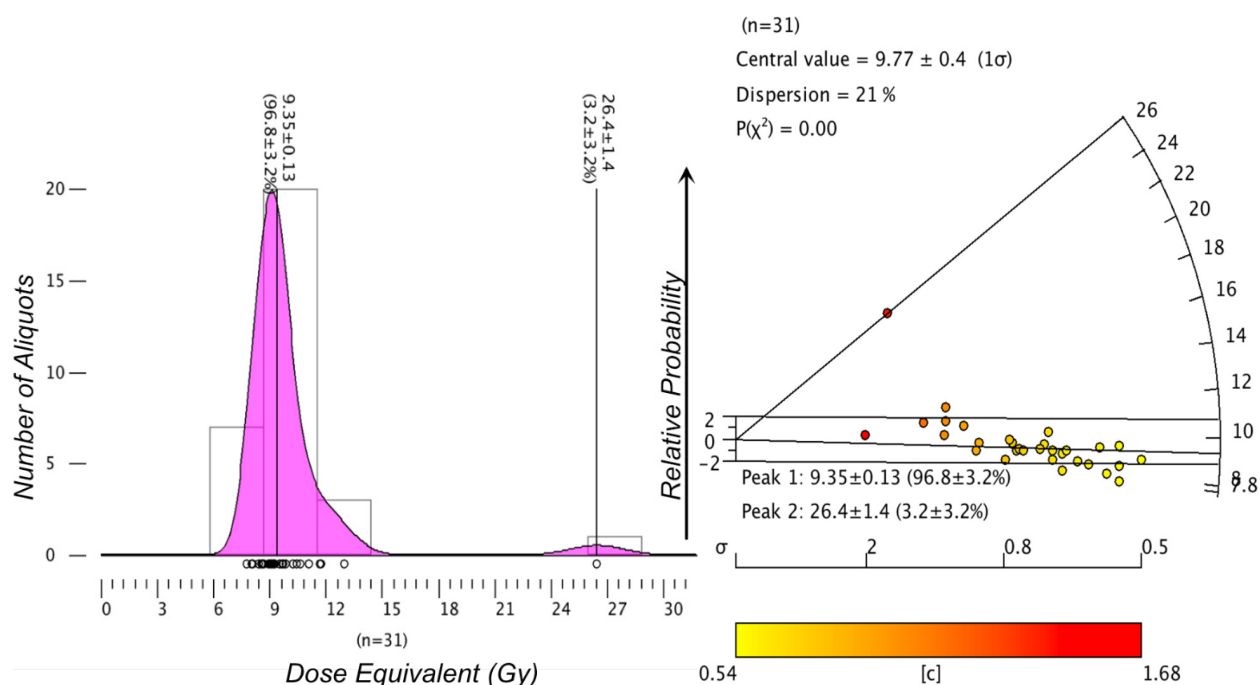


Figure S10. Relative probability histogram and radial plot for the distribution of  $D_E$  measurements in aliquots from sample 'T101'. These are IRSL measurements on feldspar grains. Yellow to red values on the scale bar [c] indicates associated uncertainty for individual  $D_E$  measurements. Age results are shown in Table 1 in the main manuscript.

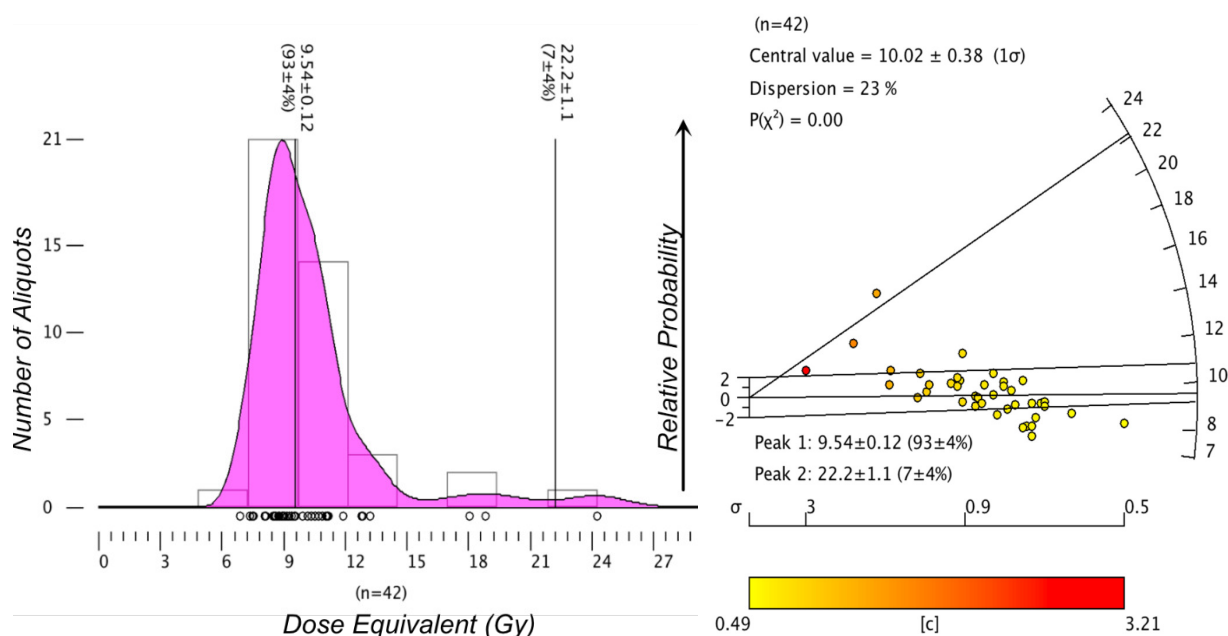


Figure S11. Relative probability histogram and radial plot for the distribution of  $D_E$  measurements in aliquots from sample 'T102'. These are IRSL measurements on feldspar grains.



Yellow to red values on the scale bar [c] indicates associated uncertainty for individual  $D_E$  measurements. Age results are shown in Table 1 in the main manuscript.

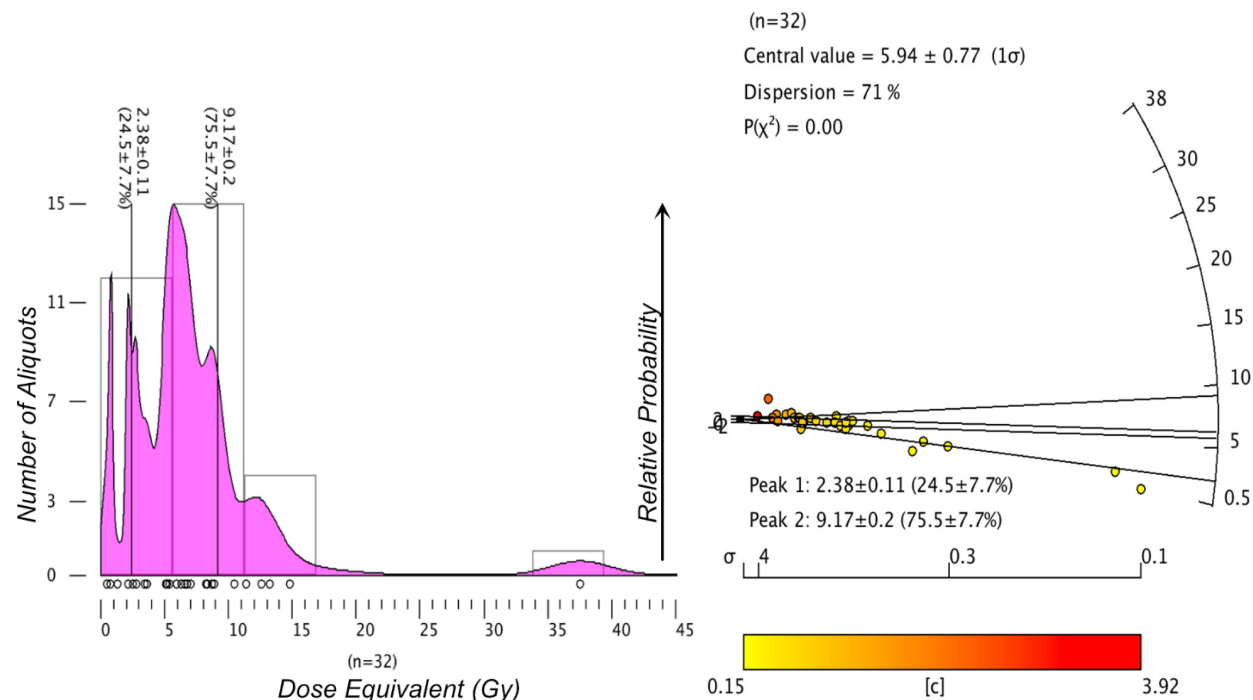


Figure S12. Relative probability histogram and radial plot for the distribution of  $D_E$  measurements in aliquots from sample 'T203'. These are BSL measurements on quartz grains, with IRSL measurements on feldspar from the same sample shown in Figure S13. Yellow to red values on the scale bar [c] indicates associated uncertainty for individual  $D_E$  measurements. Age results are shown in Table 1 in the main manuscript.

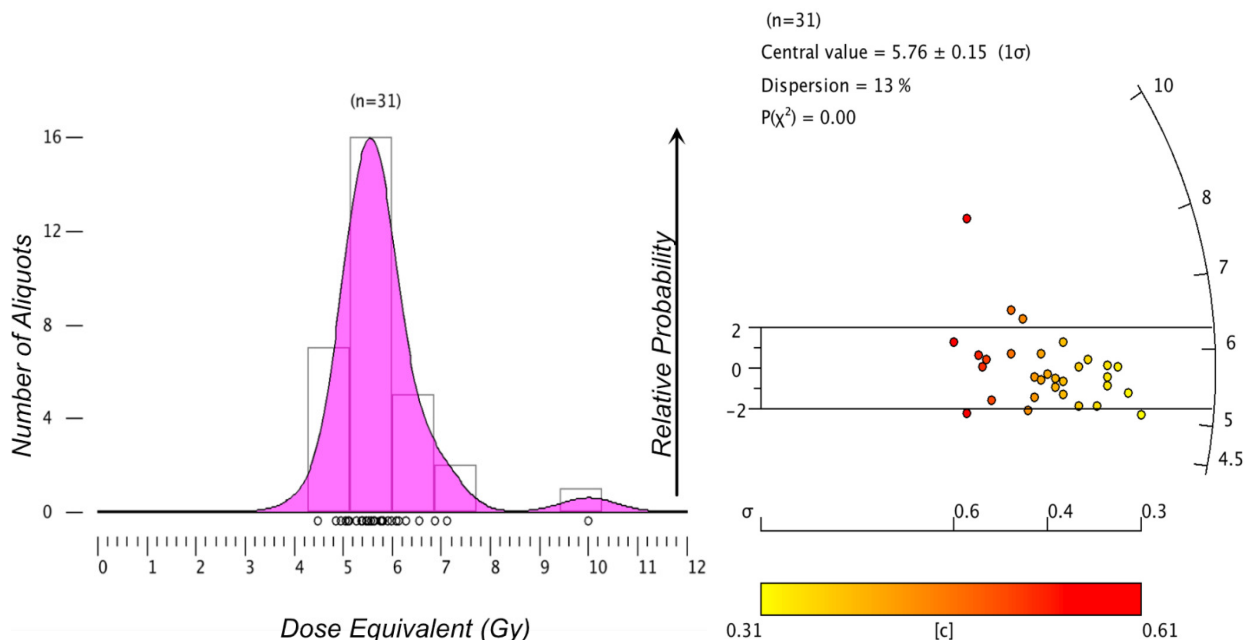




Figure S13. Relative probability histogram and radial plot for the distribution of  $D_E$  measurements in aliquots from sample 'T203'. These are IRSL measurements on feldspar grains, with BLSL measurements on quartz from the same sample shown in Figure S12. Yellow to red values on the scale bar [c] indicates associated uncertainty for individual  $D_E$  measurements. Age results are shown in Table 1 in the main manuscript.

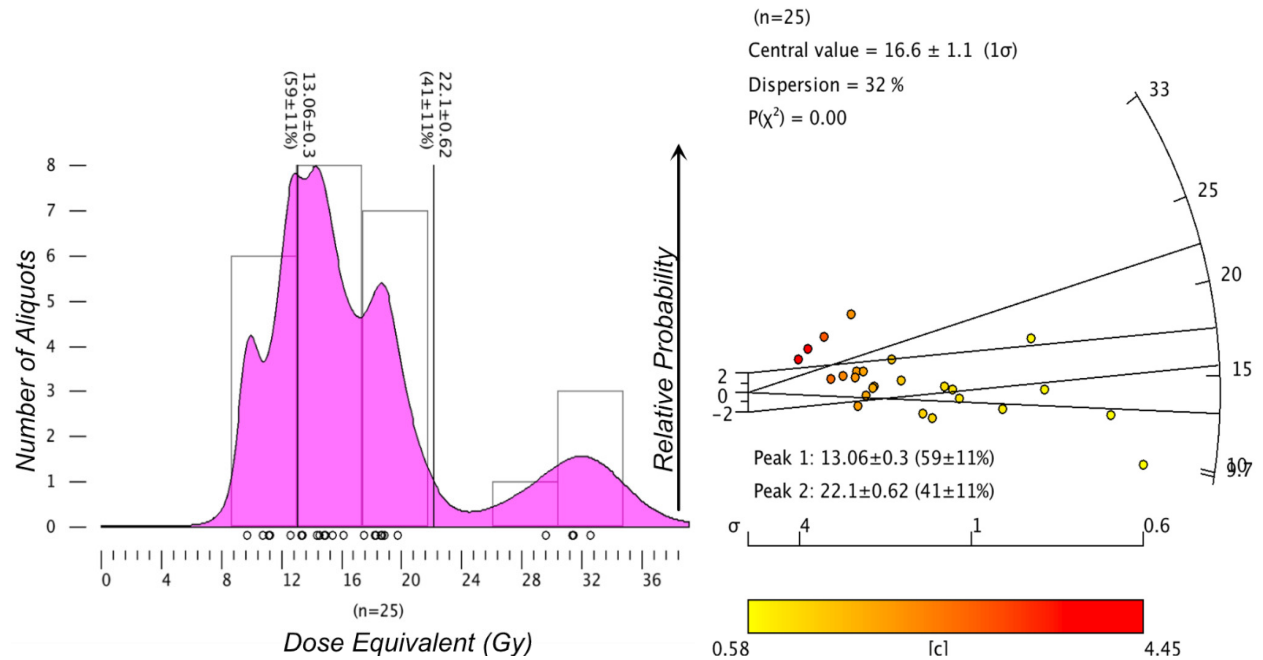


Figure S14. Relative probability histogram and radial plot for the distribution of  $D_E$  measurements in aliquots from sample 'T204'. These are BLSL measurements on quartz grains. Yellow to red values on the scale bar [c] indicates associated uncertainty for individual  $D_E$  measurements. Age results are shown in Table 1 in the main manuscript.



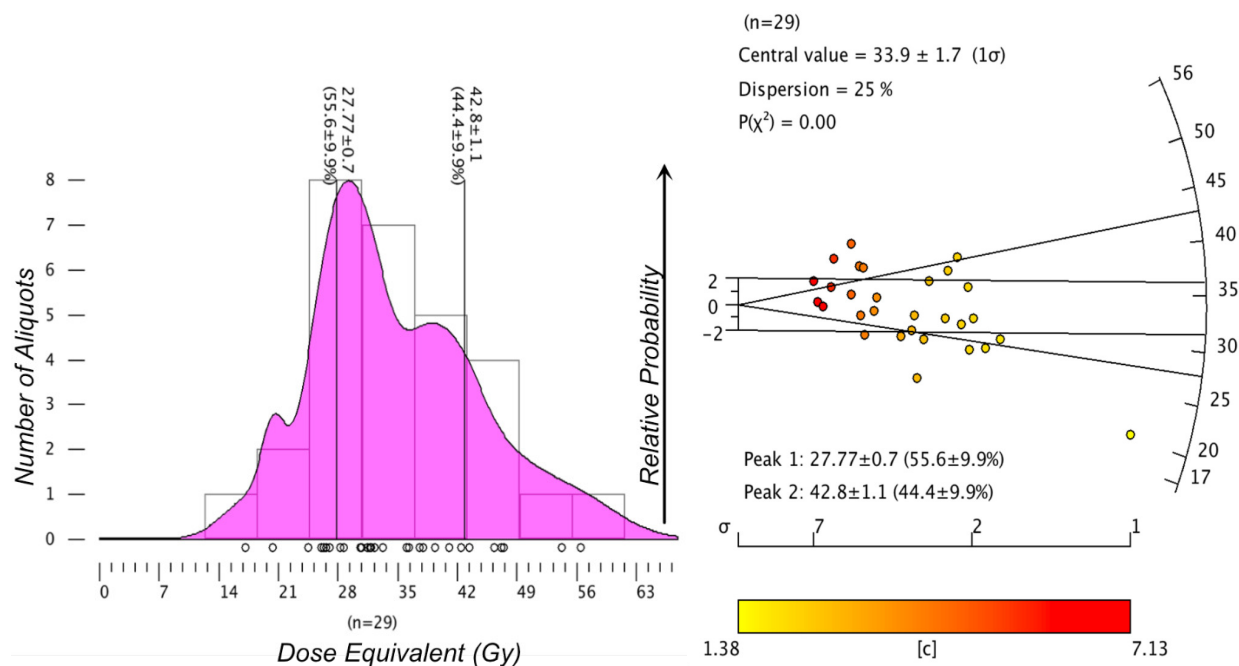


Figure S15. Relative probability histogram and radial plot for the distribution of  $D_E$  measurements in aliquots from sample 'T205'. These are BLSL measurements on quartz grains. Yellow to red values on the scale bar [c] indicates associated uncertainty for individual  $D_E$  measurements. Age results are shown in Table 1 in the main manuscript.

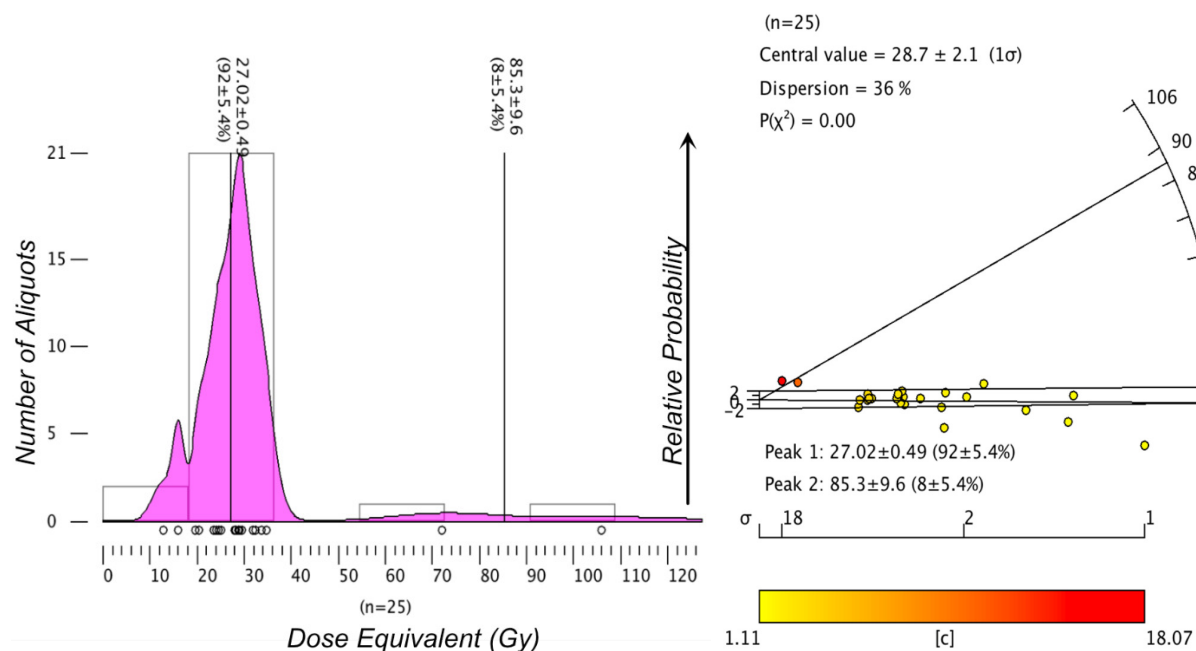


Figure S16. Relative probability histogram and radial plot for the distribution of  $D_E$  measurements in aliquots from sample 'T206'. These are BLSL measurements on quartz grains.



Yellow to red values on the scale bar [c] indicates associated uncertainty for individual  $D_E$  measurements. Age results are shown in Table 1 in the main manuscript.

#### References Cited:

- Aitken, M. J., 1998, *Introduction to Optical Dating: The Dating of Quaternary Sediments by the Use of Photon-stimulated Luminescence*, Clarendon Press.
- Durcan, J. A., G. E. King, and G. A. T. Duller, 2015, DRAC: Dose Rate and Age Calculator for trapped charge dating, *Quaternary Geochronology*, 28, 54–61, doi: [10.1016/j.quageo.2015.03.012](https://doi.org/10.1016/j.quageo.2015.03.012).
- Galbraith, R. F., 1990, The radial plot: Graphical assessment of spread in ages, *International Journal of Radiation Applications and Instrumentation. Part D. Nuclear Tracks and Radiation Measurements*, 17, no. 3, 207–214, doi: [10.1016/1359-0189\(90\)90036-W](https://doi.org/10.1016/1359-0189(90)90036-W).
- Galbraith, R. F., and P. F. Green, 1990, Estimating the component ages in a finite mixture, *International Journal of Radiation Applications and Instrumentation. Part D. Nuclear Tracks and Radiation Measurements*, 17, no. 3, 197–206, doi: [10.1016/1359-0189\(90\)90035-V](https://doi.org/10.1016/1359-0189(90)90035-V).
- Huntley, D. J., and M. Lamothe, 2001, Ubiquity of anomalous fading in K-feldspars and the measurement and correction for it in optical dating, *Can. J. Earth Sci.*, 38, no. 7, 1093–1106, doi: [10.1139/e01-013](https://doi.org/10.1139/e01-013).
- Jain, M., and Ashok. K. Singhvi, 2001, Limits to depletion of blue-green light stimulated luminescence in feldspars: implications for quartz dating, *Radiation Measurements*, 33, no. 6, 883–892, doi: [10.1016/S1350-4487\(01\)00104-4](https://doi.org/10.1016/S1350-4487(01)00104-4).
- Murray, A. S., and J. M. Olley, 2002, Precision and accuracy in the optically stimulated luminescence dating of sedimentary quartz: a status review, *Geochronometria*, Vol. 21, 1–16.
- Murray, A. S., and A. G. Wintle, 2000, Luminescence dating of quartz using an improved single-aliquot regenerative-dose protocol, *Radiation Measurements*, 32, no. 1, 57–73, doi: [10.1016/S1350-4487\(99\)00253-X](https://doi.org/10.1016/S1350-4487(99)00253-X).
- Murray, A. S., and A. G. Wintle, 2003, The single aliquot regenerative dose protocol: potential for improvements in reliability, *Radiation Measurements*, 37, no. 4, 377–381, doi: [10.1016/S1350-4487\(03\)00053-2](https://doi.org/10.1016/S1350-4487(03)00053-2).
- Porat, N., 2006, Use of magnetic separation for purifying quartz for luminescence dating, 24.
- Singhvi, A. K., and N. Porat, 2008, Impact of luminescence dating on geomorphological and palaeoclimate research in drylands, *Boreas*, 37, no. 4, 536–558, doi: [10.1111/j.1502-3885.2008.00058.x](https://doi.org/10.1111/j.1502-3885.2008.00058.x).
- Vermeesch, P., 2009, RadialPlotter: A Java application for fission track, luminescence and other radial plots, *Radiation Measurements*, 44, no. 4, 409–410, doi: [10.1016/j.radmeas.2009.05.003](https://doi.org/10.1016/j.radmeas.2009.05.003).
- Wintle, A. G., and A. S. Murray, 2006, A review of quartz optically stimulated luminescence characteristics and their relevance in single-aliquot regeneration dating protocols, *Radiation Measurements*, 41, no. 4, 369–391, doi: [10.1016/j.radmeas.2005.11.001](https://doi.org/10.1016/j.radmeas.2005.11.001).